Thermal History of the Earth: On the Importance of Surface Processes and the Size of Tectonic Plates

Cécile Grigné[1] and Manuel Combes[1]

[1]Université de Bretagne Occidentale, Institut Universitaire Européen de la Mer

November 21, 2022

Abstract

Geochemical constraints on mantle temperature indicate a regular decrease by around 250 K since 3 Ga. However models of Earth's cooling that rely on scaling laws for thermal convection without strong plates are facing a thermal runaway backwards in time, due to the power-law dependence of heat loss on temperature. To explore the effect of surface dynamics on Earth's cooling rate, we build a 2D temperature-dependent model of plate tectonics that relies on a force balance for each plate and on Earth-like parameterized behaviors for the motion, creation and disappearance of plate boundaries. While our model predicts the expected thermal runaway if plate boundaries are fixed, we obtain an average cooling rate consistent with geochemical estimates if the geometry of plate tectonics evolves through time. For a warmer mantle in the past, plates are faster but also longer (and less numerous) so that the average seafloor age and resulting heat flux always remain moderate. The predicted increase in the number of plates forwards in time is in good agreement with recent plate reconstructions over the last 400 Myr. Our model also yields plate speed and subduction area flux consistent with these reconstructions. We finally compare the effect of parameters controlling mantle viscosity and individual plate speeds to the effect of localized surface processes, such as oceanization and subduction initiation. We infer that studies of Earth's thermal history should focus on surface processes as they appear to be key control parameters.

Posted on 21 Nov 2022 — CC-BY-NC 4 — https://doi.org/10.1002/essoar.10503001.1 — This a preprint and has not been peer reviewed. Data may be preliminary.

Thermal History of the Earth: On the Importance of Surface Processes and the Size of Tectonic Plates

C. Grigné[1], M. Combes[1]

[1]Laboratoire Géosciences Océan, Université de Bretagne Occidentale-CNRS, IUEM, rue Dumont d'Urville, 29280 Plouzané, France.

Key Points:

- 2D temperature-dependent plate tectonic reorganizations are simulated over 3 Gyr
- Archean thermal catastrophe is avoided even with faster plate tectonics in the past
- Renewal of plate boundaries is key to Earth's thermal evolution over short and long timescales

Corresponding author: C. Grigné, `cecile.grigne@univ-brest.fr`

Abstract

Geochemical constraints on mantle temperature indicate a regular decrease by around 250 K since 3 Ga. However models of Earth's cooling that rely on scaling laws for thermal convection without strong plates are facing a thermal runaway backwards in time, due to the power-law dependence of heat loss on temperature. To explore the effect of surface dynamics on Earth's cooling rate, we build a 2D temperature-dependent model of plate tectonics that relies on a force balance for each plate and on Earth-like parameterized behaviors for the motion, creation and disappearance of plate boundaries. While our model predicts the expected thermal runaway if plate boundaries are fixed, we obtain an average cooling rate consistent with geochemical estimates if the geometry of plate tectonics evolves through time. For a warmer mantle in the past, plates are faster but also longer (and less numerous) so that the average seafloor age and resulting heat flux always remain moderate. The predicted increase in the number of plates forwards in time is in good agreement with recent plate reconstructions over the last 400 Myr. Our model also yields plate speed and subduction area flux consistent with these reconstructions. We finally compare the effect of parameters controlling mantle viscosity and individual plate speeds to the effect of localized surface processes, such as oceanization and subduction initiation. We infer that studies of Earth's thermal history should focus on surface processes as they appear to be key control parameters.

Plain Language Summary

The Earth's interior has been cooling over the past 3 billion years. Chemical analyses of ancient rocks show that the mantle was then about 250 degrees hotter than today, corresponding to a fairly low amount of heat released until now. However, when the mantle was hotter in the past, it was less viscous, and the dragging forces on tectonic plates were weak: plate motion was probably much faster. Heat from the Earth's interior is released mainly at oceanic ridges, where new seafloor is created. The faster the plates, the more heat is released. How so little heat has been released with significantly faster plates in the past? Several authors proposed complex phenomena playing on plate tectonics to slow down plates in the past. Here, we propose a new model including surface processes controlling plates creation and disappearance, leading to evolving plate sizes. We show that the geometry of plates is a key factor: for a hotter Earth in the past, plates were larger, so that ridges were less numerous and a moderate amount of heat was

released, even if plates were faster. This new paradigm (larger plates in the past) is compatible with observations in geological data.

1 Introduction

Reconstructing Earth's thermal history is a challenging issue: the long-standing assumption that the thermal evolution of a planet is controlled by the rheological behavior of its interiors (e.g. Tozer, 1967; Davies, 1980; Nataf & Richter, 1982) cannot be reconciled with petrological and geochemical constraints on mantle temperature in the past. Earth's thermal evolution is commonly studied by a global heat balance between secular cooling, internal heat production H due to a radioactive decay and surface heat loss Q:

$$Mc_p \frac{dT_m}{dt} = H(t) - Q(T_m), \tag{1}$$

where T_m is the mantle potential temperature, M the mass of the Earth, and c_p its average thermal capacity, accounting for the isentropic thermal gradient in the mantle and the coupling with core, assuming that mantle and core have similar cooling rates (e.g. Korenaga, 2008). In order to integrate Eq. 1, a first approach consists in using a simple convective scaling law for the heat flow Q as a function of the mantle temperature T_m. Such a scaling is usually derived from thermal boundary layer considerations and laboratory or numerical experiments with an isoviscous fluid (e.g. Howard, 1966) and is written in a dimensionless form as $Nu \sim Ra^{1/3}$, where Nu is the dimensionless heat flux (Nusselt number) and Ra the Rayleigh number of the fluid. As the viscosity of the mantle is highly temperature-dependent (e.g. Karato & Wu, 1993), this scaling implies that the heat flow Q increases exponentially with the mantle temperature T_m, which results in unacceptably high temperatures in the past, implying a totally molten upper mantle in the late Archean (e.g. Davies, 1980; Schubert et al., 1980; Richter, 1985). Abbott et al. (1994) inferred from compositional variations of mid-oceanic ridge basalts that mantle temperatures have decreased by about 150 K since the Archean. Herzberg et al. (2010) studied non-arc basalts of late-Archean and Proterozoic age and obtained a maximum potential temperature about 200-250 K higher than the present one at 3 Ga.

To obtain these reasonable temperatures in the past, several strategies were proposed. First, the relative importance of radiogenic heating compared to heat loss, known as the Urey ratio $Ur = H/Q$, plays a major role in the cooling rate (Eq. 1): a high value of Ur helps avoid the Archean thermal catastrophe (e.g. Davies, 1980; Schubert et al.,

1980) but is inconsistent with geochemical estimates of Earth composition (e.g. Korenaga, 2008). A layered mantle in the past could also slow down mantle's cooling (e.g. Honda, 1995; Butler & Peltier, 2002) but the role of the endothermic phase change between the lower- and upper-mantle needs to be exaggerated (Korenaga, 2008). Adding the thermal insulating effect of continents and/or the effect of continental growth on mantle depletion can help prevent a drastic thermal runaway (e.g. Grigné & Labrosse, 2001; Lenardic et al., 2011), but the obtained cooling rates are still decreasing with time which is not consistent with geochemically derived temperature estimates (Herzberg et al., 2010).

These previous approaches consider a convective scaling for the heat flow Q as a function of mantle temperature and viscosity in the form $Nu \sim Ra^{1/3}$. Another approach consists in lowering the dependence of Nu on Ra. Conrad and Hager (1999) proposed that the main viscous resistance to mantle convection comes from the bending of the oceanic lithosphere at subduction zones, which renders plate motion less dependent on the viscosity of Earth's interior than a simple convective approach. This idea was explored by Sleep (2000) and Korenaga (2003, 2006) to propose thermal evolution models where higher temperatures in the past result in slower plates and a reduced heat loss. However, if the correct "bending length" is used in convection models with plate tectonics (Ribe, 2010), the Archean thermal runaway cannot be avoided by bending dissipation only (Gerardi et al., 2019). Korenaga (2011), using a scaling derived from numerical experiments with strong plates (Korenaga, 2010), proposed a model of Earth thermal evolution, taking into account the dehydration of the lithosphere through mid-ocean ridges melting, which stiffens the oceanic lithosphere, the possible mantle hydration over time from slab subduction, which has an important role on mantle viscosity (e.g. Hirth & Kohlstedt, 1996; Mei & Kohlstedt, 2000), as well as continental growth for the computation of the mantle radiogenic heat production. This model is consistent with geochemical estimates of temperature, but the derived average plate speeds cannot be reconciled with recent models of plate reconstructions. In his preferred model, Korenaga (2011) obtains a median speed decreasing from $\sim$4 cm/yr at present to around 3$\pm$1 cm/yr at 2.5 Ga, and the maximum value of the 95th percentile since the Archean is less than 4.5 cm/yr at around 500 Ma. This is in contradiction with the two independent models of plate reconstructions that go back to Paleozoic, which both suggest average plate speed over 8 cm/yr at 500 Myr, with possible peaks of more than 12 cm/yr in the Paleozoic (Vérard et al., 2015; Young et al., 2019). Going further back in time, paleomagnetic data showing rapid changes in relative paleolatitudes between individual cratons suggest possible peaks of fast plate motion (from 10 to 100 cm/yr) around 1.1, 2.0 and 2.7 Ga (O'Neill et al., 2007), which is also not compatible with continously slow plates before 500 Ma as suggested by Korenaga (2011). This example illustrates that most models of Earth's thermal evolution discuss temperature as a function of time in comparison to geochemical estimates, but plate speed, in comparison to geological data and reconstructions, is rarely considered. Another problem is that most Earth's thermal models do not reflect some important terrestrial observations: not all plates are driven by subduction, strong heat flux variations are coeval with ridge creation or subduction initiation, and fast or slow or even immobile plates coexist (present-day plate velocities vary by a factor of 40 (e.g. Argus et al., 2011)).

The rate of assembly and dispersal of supercontinents (e.g. Pisarevsky et al., 2014; Condie et al., 2015; Evans et al., 2016) or the lifetime of passive margins (Bradley, 2008) in the Proterozoic are used as information regarding the past rhythm of plate tectonics. Condie et al. (2015) infer that the decreasing lifespan of passive margins and the increase in the number of orogens with time suggest that plates were slower in the past, as proposed by Korenaga (2003, 2006, 2011). But a direct relation between the tempo of such tectonic events and the speed of plates would imply that the size of plates did not change through time. However, plate reconstructions suggest an increase in the number of plates since 400 Ma (Matthews et al., 2016), which is consistent with numerical models of mantle convection with strong plates (Mallard et al., 2016) (see Discussion in section 4 here). It is then interesting to note that fewer and larger plates in the past may also account for the apparent ”slow” past tempo of tectonics events.

In the present study, we look into Earth's thermal evolution with aiming at explaining not only past moderate cooling rates, but also past plate speeds and rates of tectonic events such as continental collisions. We use a 2D model of plate tectonics (MACMA: Multi-Agent Convective Mantle) (Combes et al., 2012) based on a force balance for each plate and on empirical parameterizations to treat local plate reorganizations. The model includes mobile plate boundaries that can collide, vanish or be created, asymmetric subduction zones and their consequent overriding plates, together with breakable insulating continents, bordered by active or passive margins. With this approach, the geometry of plate tectonics is not fixed but free to adapt as the temperature and plate speeds evolve. Combes et al. (2012) conducted several experiments that yielded moderate cooling rates comprised between 55 and 110 K/Gyr over the past 3 Gyr, but the initial conditions and the main parameters of the model were not varied on a wide range of possibilities. Here, we present a full analysis of Earth's thermal evolutions obtained with this approach, and compare them with numerous available geochemical and geological data. Our results with fixed plate boundaries exhibit the same thermal catastrophe as the one arising in classical parameterized studies of Earth's thermal history. With evolving plate boundaries, conversely, the obtained thermal evolution over 3 Gyr is in good agreement with terrestrial estimates by Herzberg et al. (2010). Plate speed, slab flux and the number of plates also correspond to recent tectonic reconstructions over the Phanerozoic (Vérard et al., 2015; Matthews et al., 2016; Hounslow et al., 2018; Young et al., 2019). The obtained rate of collisions between continents is also slightly increasing over time, as suggested by Condie et al. (2015). These results, consistent with geochemical and geological data while plate speed is still simply controlled by the mantle viscosity and decreasing with time, are the consequences of the surface processes (subduction initiations and cessations, and continental cycles) included in our model, that control the evolving geometry of plate tectonics.

2 The MACMA Model

The MACMA (MultiAgent Convective MAntle) framework is a 2D planet covered by mobile plates, with evolving plate boundaries that can be created and eliminated. The conservation of heat is written as Eq. 1, using a uniform temperature for the mantle. Mass and momentum conservations are imposed with a force balance for each plate, considering a total of 3 driving forces and 3 resistive forces. The general framework of MACMA is presented in Figure 1. Plate boundaries are ridges and trenches that can both migrate through the oceans. Other elements are continents and staples, which are discontinuities in oceanic lithosphere ages appearing when two plate boundaries collide.

Plate velocities are deduced from a force balance, using a layered mantle (lithosphere, upper mantle and lower mantle). Each layer has a newtonian temperature-dependent viscosity, written as an Arrhenius law using reference values for present-day Earth. Hereafter, the subscript 0 stands for present-day values:

$$\eta_i(T_m) = \eta_{i_0}\ \exp\left(\frac{E}{R}\left(\frac{1}{T_m} - \frac{1}{T_{m_0}}\right)\right). \tag{2}$$

The subscript i stands for the different layers in Earth (i = pl, um or lm for oceanic plates, upper mantle and lower mantle respectively), E is the activation energy and $R = 8.314$ J.K^{-1}.mol^{-1}

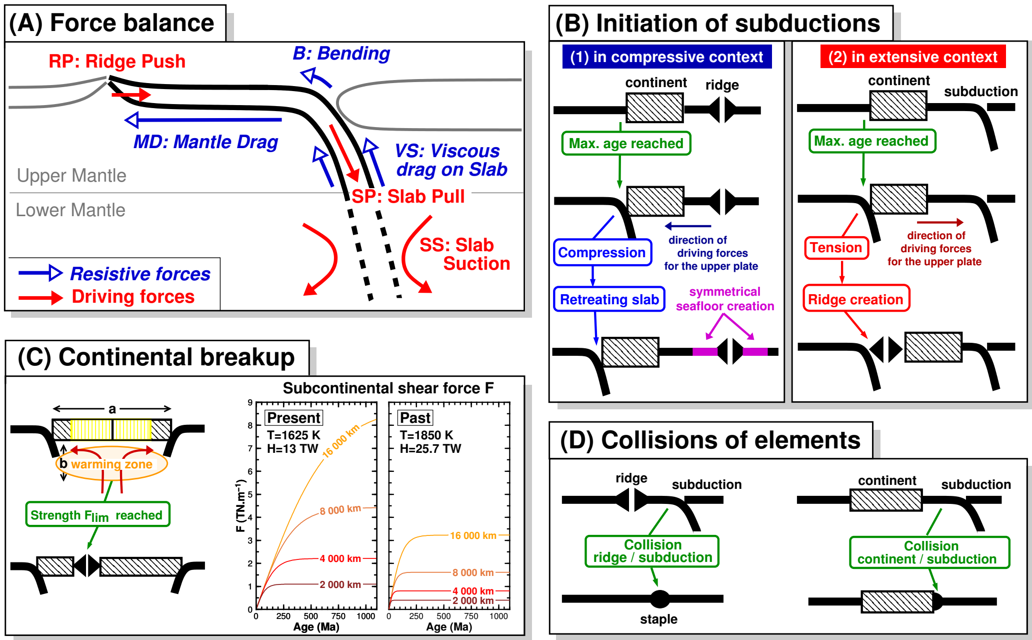

Figure 1. (A) Force balance used in this study. (B) Initiation of subductions in compressive (B1) and extensive context (B2). When the ocean seafloor age at the passive margin reaches the limit age $\tau_{\rm subd}$, a subduction is created. The compressive case (B1) occurs when the overriding plate moves towards the trench. The symmetrical accretion around the ridge is also schematized. The extensive case (B2) occurs when the overriding plate moves away from the trench: a ridge is created to compensate for the diverging motion of the two plates. (C) Continental breakup: an advective shear force F below the continent is computed and compared to a fixed continental strength $F_{\rm lim}$. If $F > F_{\rm lim}$ the continent can open, at a position that is randomly picked in the yellow zone (middle of continent $\pm$ 1/3 of its width a). The subcontinental shear force F (see appendix B) is represented as a function of the age of the continent and of its width a (a=2000, 4000, 8000 or 16000 km). For this computation at present day, the viscosity of the upper mantle is $\eta_{\rm um} = 10^{21}$ Pa.s (for T=1625 K) and the radiogenic heat production is $H = 13$ TW. For past hotter conditions (chosen to represent the late Archean), we use $H = 25.7$ TW and $\eta_{\rm um} = 6.7 \times 10^{19}$ Pa.s (for T=1850 K, using the activation energy E=300 kJ.mol^{-1}). (D) Processes for plate boundary eliminations and creations of staples.

is the gas constant derived from the Boltzmann distribution. Parameters used in this study are given in Table 1.

The thickness of plates δ as a function of the seafloor age τ is needed in the expressions of several forces hereafter. From the halfspace cooling model (e.g. Turcotte & Schubert, 2002), we use

$$\delta(\tau) = c\sqrt{\kappa\tau} \tag{3}$$

with κ the thermal diffusivity. We use the prefactor $c = 2.1$ yielding an oceanic lithospheric thickness of ~10 km for $\tau = 1$ Myr and ~95 km for $\tau = 80$ Myr. A small scale convection (SSC) mechanism can be used as an option in the MACMA model, in order to limit seafloor thickness after a critical age (for details, see Combes et al. (2012)).

2.1 Force Balance

The force balance used in this study is presented in Figure 1A. With a 1D geometry for plates, we express the forces in N.m^{-1}.

2.1.1 Driving Forces

The driving forces are the following: (1) ridge push (RP), (2) slab pull (SP) and (3) slab suction (SS).

Following Parsons and Richter (1980), we write

$$\mathrm{RP} = \alpha\rho g \, (T_m - T_s) \, \kappa\tau_{\max} \tag{4}$$

where $\tau_{\max}$ is the maximum age of the plate, α the thermal expansivity and $T_m - T_s$ the thermal jump across the lithosphere.

Slab pull is due to the excess weight of the cold slab, and we consider this force in the upper mantle only, as was done by Conrad and Lithgow-Bertelloni (2002) and Conrad and Lithgow-Bertelloni (2004):

$$\mathrm{SP} = \Delta\rho \; g \; \delta(\tau_{\max}) \; \min(Z, d_{\mathrm{um}}), \tag{5}$$

where Z is the depth reached by the slab and $\delta(\tau_{\max})$ is the thickness of the slab (Eq. 3).

Following Conrad and Lithgow-Bertelloni (2002, 2004), we consider slab suction (SS) in the lower mantle: descending slabs induce mantle flow that pulls both the subducting and the overriding plates towards the subduction zone. SS is expressed as a shear

Table 1. Parameters used in this study. In bold font are the parameters used for the reference case (see section 3.3). Their effects are studied in section 3.4.

Parameter	Symbol	Value	
Earth's mass	M	5.98×10^{24}	kg
Mantle's mass	M_{m}	4.08×10^{24}	kg
Continental crust's mass	M_{cont}	2.20×10^{22}	kg
Earth's radius	R_{E}	6370	km
Upper mantle thickness	d_{um}	670	km
Lower mantle thickness	d_{lm}	2230	km
Gravitational acceleration	g	10	$\mathrm{m.s^{-2}}$
Thermal expansivity	α	2×10^{-5}	$\mathrm{K^{-1}}$
Upper mantle density	ρ	3300	$\mathrm{kg.m^{-3}}$
Slab density contrast	$\Delta\rho$	65	$\mathrm{kg.m^{-3}}$
Present-day oceanic lithosphere viscosity	η_{pl_0}	$\mathbf{1.25 \times 10^{23}}$	**Pa.s**
Present-day upper mantle viscosity	η_{um_0}	$\mathbf{5 \times 10^{20}}$	**Pa.s**
Present-day lower mantle viscosity	η_{lm_0}	$\mathbf{5 \times 10^{22}}$	**Pa.s**
Activation energy	E	**350**	$\mathbf{kJ.mol^{-1}}$
Oeanic lithosphere thermal conductivity	k	3	$\mathrm{W.m^{-1}.K^{-1}}$
Thermal diffusivity	κ	8×10^{-7}	$\mathrm{m^2.s^{-1}}$
Earth's average thermal capacity	c_p	1200	$\mathrm{J.kg^{-1}.K^{-1}}$
Surface temperature	T_s	273	K
Present-day mantle potential temperature	T_{m_0}	1625	K
Present-day slabs Stokes velocity in the lower mantle	V_{s_0}	1	cm/yr
Present-day critical age for subduction initiation	τ_{subd_0}	**180**	**Myr**
Minimum radius of curvature of plates	R_{min}	300	km
Continental strength	F_{lim}	**2**	$\mathbf{TN.m^{-1}}$
Subcontinental warming zone thickness	b	350	km

stress exerted on the slab and transmitted to the horizontal plates on both sides of the trench:

$$\mathrm{SS} \;=\; \eta_{\mathrm{lm}_0} \left(\frac{V_{s_0}}{4\ d_{\mathrm{lm}}} \right) \ \max(0, Z - d_{\mathrm{um}}) \tag{6}$$

Only the height of the slab in the lower mantle is considered here. V_{s_0} is the present-day vertical velocity of the slab in the lower mantle, described as a Stokes velocity (Guillou-Frottier et al., 1995; Griffiths et al., 1995; Goes et al., 2011), so that at each time we have $\eta_{\mathrm{lm}}\ V_s = \eta_{\mathrm{lm}_0}\ V_{s_0}$. Eq. 6 is therefore written with present-day values. Considering a fluid loop model (e.g. Grigné et al., 2005), we make the rough approximation that only a quarter of the drag force of the sinking slab results in suction on each horizontal plate above the plate (factor 4 in Eq. 6). The amplitude of SS is controlled by the choice for the value of V_{s_0}. The factor $1/(4\ d_{\mathrm{lm}})$ in Eq. 6 yields present-day plate speeds consistent with observations when we choose a value for V_{s_0} also consistent with recent estimates of the descent rate of slabs in the lower mantle (see section 2.1.3).

The three driving forces RP, SP and SS depend on the depth of slabs and on seafloor ages, but not on the velocities of plates. SP is taken into account only for subducting plates, while SS is considered for both the subducting and the overriding plates.

2.1.2 Resistive Forces

The resistive forces are: (1) the vertical shear stress on the slabs in the upper mantle (VS), (2) the horizontal mantle drag under the plates (MD) and (3) the bending force (B) (see Figure 1A). They can all be expressed as shear forces, equal to the product of an effective viscosity that accounts for the geometry of the plate, and of the velocity U of the plate. The equivalent viscosities are denoted hereafter by η_{VS}, η_{MD} and η_{B} and their expressions are given in appendix A. The sum of the resistive forces is

$$\mathrm{VS} + \mathrm{MD} + \mathrm{B} = \ - \left(\eta_{\mathrm{VS}} + \eta_{\mathrm{MD}} + \eta_{\mathrm{B}}\right)\ U \tag{7}$$

2.1.3 Plate Velocity Computation and Choice for Present-day Parameters

Considering a mantle with infinite Prandtl number, the forces exerted on each plate cancel out, which allows to calculate each plate velocity as:

$$U = \frac{\mathrm{RP} + \mathrm{SP} + \mathrm{SS}}{\eta_{\mathrm{MD}} + \eta_{\mathrm{VS}} + \eta_{\mathrm{B}}} \tag{8}$$

The parameters entering the expressions for the different forces are given in Table 1. We focus the discussion here on the choice for the descent rate of slabs V_{s_0} (entering the expression of SS) and on the present-day viscosities for the lower mantle η_{lm_0}, the upper mantle η_{um_0} and the oceanic plates η_{pl_0}, entering the expressions of the resistive forces and their equivalent viscosities η_{MD}, η_{VS} and η_{B}. V_{s_0} is estimated from seismic tomography to be between 1 and 2 cm/yr (Van der Meer et al., 2010, 2018; Čížková et al., 2012; Domeier et al., 2016). In numerical models of a subducting slab in a convective system, this range of velocity can be obtained if the viscosity of the lower mantle is comprised between 10^{22} and 10^{23} Pa.s (e.g. Kaneko et al., 2019). Geoid and postglacial isostatic adjustments studies, as well as instantaneous models of mantle circulation coupled to lithospheric plates, suggest that the lower mantle is about 100 times more viscous than the upper mantle (e.g. Faccenda & Dal Zilio, 2017). We therefore choose for the reference model $V_{s_0} = 1$ cm/yr, $\eta_{\mathrm{lm}} = 5 \times 10^{22}$ Pa.s and $\eta_{\mathrm{um}} = 5 \times 10^{20}$ Pa.s. For the bending force, we choose a minimum radius of curvature of plates (at the trench) R_{min} =300 km and a lithosphere 250 times more viscous than the upper mantle (Wu et al., 2008; Holt et al., 2015; Behr & Becker, 2018): $\eta_{\mathrm{pl}_0} = 1.25 \times 10^{23}$ Pa.s.

These parameters yield reasonable plate speeds for present time (see Figure 2). We do not aim at obtaining precise velocities that could be directly compared to actual plates for the present-day Earth, but we are checking here that the force balance gives reasonable speeds, with a few typical Earth features: plates driven by significant slab pull are at least thrice faster than non-subducting plates, and there is no direct relation between plates' sizes and their speeds, aside from the observation that plates with speeds larger than 0.75 deg.Myr^{-1} all have an area smaller than 0.15 steradians (e.g. Forsyth & Uyeda, 1975; Argus et al., 2011).

Figure 2 shows that for six terrestrial plates whose geometry can be relatively well described in a 2D frame, all bounded by a ridge and a trench (either as the subducting plate or the overriding plate), our force balance yields reasonable results. The speeds of four subducting plates (Juan de Fuca, JF; Cocos, CO; Nazca, NZ and Pacific, PA) can be approximately explained through Eqs. 4 to 8 by their different sizes and variable maximum ages at the trench. The obtained differences between these subducting plates and two non-subducting plates (North America, NA and South America, SA) are also correct. Note that the age at the trench and the depth of the slab that are considered for these two non-subducting plates are the values for the plates that NA and SA are over-

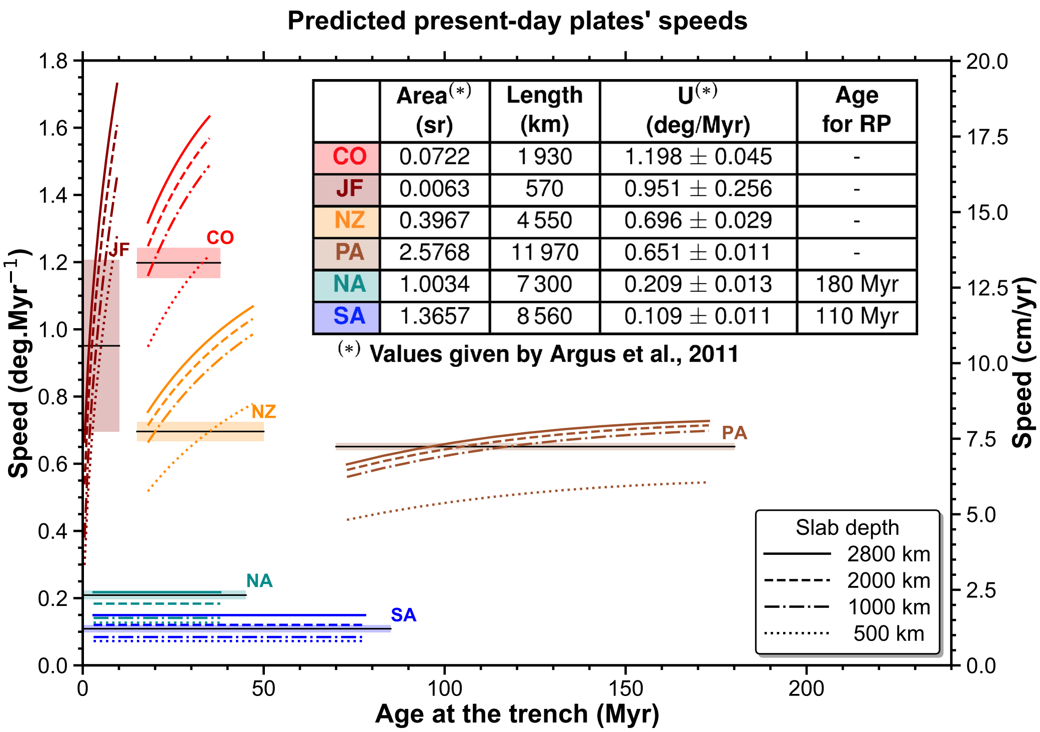

Figure 2. Plate velocities obtained with the force balance given by Eq. 8 (black curves), for different ages at the trench (horizontal axis) and different depths reached by the slab. We test sizes of plates corresponding to Juan de Fuca (JF), Cocos (CO), Nazca (NZ), Pacific (PA), North America (NA) and South America (SA). Velocities given by Argus et al. (2011) are shown with horizontal lines and their corresponding 95% confidence limits with shaded area. The length of plates is $L = 2\ R_{\mathrm{E}}\ \arccos\big(1 - A/(2\pi)\big)$ where R_{E} is Earth's radius and A the plate area in steradians. The range of ages at the trench tested for each plate is deduced from the oceanic ages map of Müller et al. (2008). For the ridge push force of non-subducting plates, we consider the following ages at the Atlantic passive margins: 180 Myr for NA and 110 Myr for SA.

riding (PA and NZ, respectively). Their own maximum oceanic ages is considered for the term of ridge push (RP) only. The older ages on the Atlantic margins for NA compared to SA and the fact that NA is overriding younger plates than SA, resulting in lower resistive forces $|VS|$ and $|B|$, can explain the larger value observed for NA.

2.2 Dynamics of Plate Boundaries

2.2.1 Velocity of Trenches and Ridges

Simple laws are used to account for the mobility of plate boundaries (see Figure 1B). Trenches are given the velocity of their overriding plates, which undergo the resistive forces acting on the slab. Only plates limited by two ridges have $\eta_{\mathrm{VS}} = \eta_{\mathrm{B}} = 0$. As for ridges, we consider symmetric spreading: ridges are given a velocity equal to half the sum of the velocities of the two diverging plates.

2.2.2 Elimination of Plate Boundaries

When collisions occur between two plate boundaries (trench-ridge or trench-trench), both of them disappear and are replaced by a so-called staple, which marks a former plate boundary that becomes an age discontinuity in the middle of a plate upon collision (see Figure 1D).

2.2.3 Creation of New Ridges

New ridges may be created in two circumstances: when tension appears on an overriding plate in a subduction zone, and during continental break-up. The former case is illustrated in Figure 1B: when the overriding plate is driven away from the trench, we impose the creation of a new ridge which represents a simplified back-arc basin.

Continental break-up is shown in Figure 1C: we consider that continents have an insulating effect (e.g. Gurnis, 1988; Guillou & Jaupart, 1995; Coltice et al., 2007; Grigné et al., 2007; Rolf et al., 2012; Whitehead & Behn, 2015), which in turn enhances convective vigor in the upper mantle (e.g. Lenardic et al., 2005; Samuel et al., 2011). We derive a parameterization of the warming rate and subsequent advective motion in a shallow layer below a continent as a function of its width and of the radiogenic heating rate in the mantle. The resulting shear force F, which also depends on mantle viscosity, has to overcome a fixed yield strength $F_{\rm lim}$ in order for the continent to break up (see Combes et al. (2012) and appendix B for calculation details). This simplified oceanization parameterization does not reflect complex interactions between continents and mantle flow (e.g. O'Neill et al., 2009) but yields a physically reasonable behavior as a function of T_m: (1) a plateau in the shear force F is reached after a transient period lasting a few hundreds of Myr (see Figure 1C), (2) wider continents induce larger shear forces F and are therefore breaking more easily than narrow continents, (3) there is a minimum width for a continent to break, which depends on the chosen value of $F_{\rm lim}$ and on the thermal state of the mantle, and (4) because of a lower viscosity in a hotter mantle, the shear force F after a given duration and for a given continental width was lower in the past, implying that the minimum size for a continent to break was larger in the past.

In their numerical experiments, Heron and Lowman (2014) obtained thermal anomalies at high Rayleigh number beneath continents extensively ringed by subduction zones. In our model, continental break-ups occur only if the plate that contains the continent is limited by at least one subduction zone. The slab direction and position do not matter, i.e. it is not required that the continent is bordered by an active margin. Without this condition in our 2D setting, the new ridge created by continental break-up, which exhibits initially a null ridge push force (seafloor of age zero), would immediately reclose because of the two opposing ridge push forces on either side of the plate. Furthermore, in order to avoid symmetrical configurations that may arise from breaking up the continent right in its middle, the rifting position is randomly chosen (see Figure 1C). Our results show temperature anomalies around +15 K, in good agreement with numerical experiments by Yoshida (2013).

2.2.4 Creation of New Subductions

Many processes have been proposed for the initiation of subduction (e.g. McKenzie, 1977; Cloetingh et al., 1989; Mueller & Phillips, 1991; Gurnis et al., 2004; Crameri & Kaus, 2010; Nikolaeva et al., 2011; Levy & Jaupart, 2012), but no analytical formulation can be integrated at a global scale to simulate a starting mechanism (Gerya & Meilick, 2011). Here, without considering the mechanical details of seafloor destabilization, we make the assumption that subduction initiation occurs at a certain critical age $\tau_{\rm subd}$, when the negative buoyancy of the oceanic lithosphere exceeds a critical yield strength σ_y which is considered as a constant over time. This negative buoyancy is proportional to $\alpha\rho g(T_m - T_s)\ \delta(\tau)$. Expressing the lithospheric thickness δ as a function of the seafloor age τ (Eq. 3) and equating the critical buoyancy (proportional to $\sqrt{\tau_{\text{subd}}}$, where τ_{subd} denotes the critical age for subduction initiation) at any age to the present-day one, the destabilization occurs when

$$\tau_{\text{subd}}(T_m) = \tau_{\text{subd}_0} \left(\frac{T_{m_0} - T_s}{T_m - T_s} \right)^2 \tag{9}$$

where τ_{subd_0} is the present-day age for the initiation of subduction, chosen at 180 Myr in our reference case. An additional condition is used: subductions are created only at discontinuities in lithospheric ages (passive margins and staples). It is important to note that the critical age of subduction τ_{subd} is temperature-dependent, which allows the system to adapt its surface behavior to the mantle thermal evolution. τ_{subd} =156 and 137 Myr when the temperature is increased by 100 and 200 K, respectively.

2.3 Thermal Balance and Time Evolution

The age of the oceanic lithosphere is tracked using a resolution of 0.25° (27.8 km). New age points are created at ridges, and they are consumed by subduction. At each time step and for every point of the oceanic lithosphere, the seafloor age τ is used to compute the local heat flux $q_{\text{loc}}(\tau)$:

$$q_{\text{loc}}(\tau) = \frac{k\ (T_m - T_s)}{\sqrt{\pi\kappa\ \tau}}. \tag{10}$$

This is integrated over the oceanic surface to compute the total heat flow Q. To convert from an angular distance β in our 2D setting to a surface area, we consider that our geometry is a great circle slice of Earth and that each plate is a spherical biangle, whose surface area is then $A = 2\beta\ R_E^2$. Continents are considered as perfectly insulating and have a constant total area equal to 40% of Earth's surface. Mantle temperature T_m is updated using Eq. 1. For the internal radiogenic heat $H(t)$, we consider present-day depletion throughout Earth's history: continents have a constant total mass M_{cont}. Depleted mantle concentrations in the radiogenic isotopes of U, Th and K are then computed using concentrations in the bulk silicate Earth given by McDonough and Sun (1995) and concentrations in the continental crust given by Rudnick and Gao (2003). Internal heat from radioactive origin then decreases from 31.2 TW at 3 Ga to 13.0 TW at present.

An explicit method is used for the time evolution of the model. First, each point (oceanic ages, plate boundaries, staples and continental borders) is advanced using its velocity and a time step dt equal to or less than 5000 years, limited so that no point is moved by more than half the resolution, equal to 0.25°, which is equivalent to applying a Courant-Friedrichs-Lewy condition with a Courant number equal to 0.5. If a collision between two plate boundaries should occur over one time step, dt is again reduced so that a perfect collision is reached without any overlap between elements. A finite difference form of Eq. 1 is used to update T_m, and new temperature-dependent viscosities are computed. Driving and resistive forces are updated using the new positions and viscosities. The plate speed calculation (Eq. 8) and the criteria described in section 2.2 are then used to move points for the next time step.

3 Results

3.1 Fixed Plate Boundaries

3.1.1 Temperature Evolution

All simulations presented in this section are started with an even number of equal-sized oceanic plates, all limited by a ridge and a trench where the seafloor age is initially $\tau = 10$ Myr. Continents are not allowed to break up. With these symmetrical initial configurations, all plate boundaries remain perfectly fixed and the thermal evolution is controlled entirely by the speed of permanently subducting plates, itself controlled by temperature-dependent viscosities. More than 150 experiments were carried out with fixed boundaries, initial temperatures ranging from 1700 to 2000 K and initial ages from 400 Ma to 3.0 Ga. We present in Figure 3 only initial states that yield a temperature of 1625 K at present-day.

Petrological estimates of the mantle potential temperature of Herzberg et al. (2010) are shown with yellow circles in Figure 3(e). We use MgO contents for non-arc basalts given by Herzberg et al. (2010) and the relation between the mantle potential temperature and MgO contents given by Herzberg and Asimow (2015). These authors indicate that the uncertainty on MgO contents translates into a possible error of ±42 K on the obtained mantle potential temperatures. The thermal evolutions that we obtain with fixed plate boundaries exhibit the typical runaway shape and are clearly impossible to reconcile with those estimates.

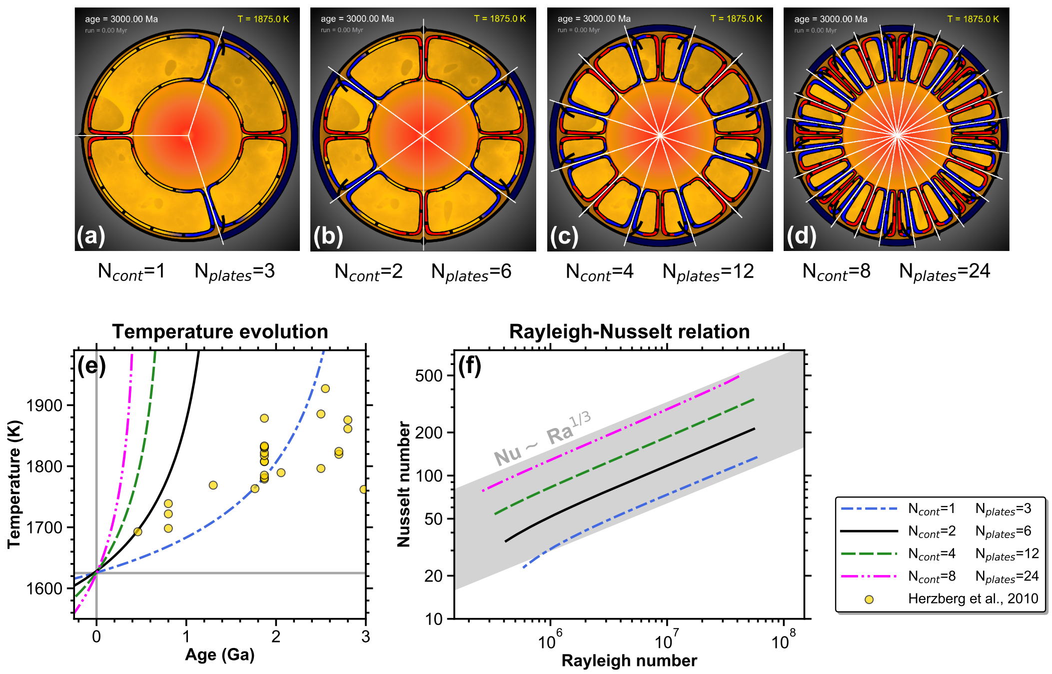

Figure 3. Configurations with fixed plate boundaries (a, b, c and d) and thermal evolution obtained with these configurations (e). Estimates of mantle potential temperatures derived from MgO contents by Herzberg et al. (2010) are shown as yellow circles. We use the relation $T_m(K) = 1298 + 28.6\ \mathrm{MgO} - 0.084\ \mathrm{MgO}^2$ given by Herzberg and Asimow (2015). (f) Dimensionless representation of the obtained heat flow $Q(T_m)$ as Nusselt number Nu vs. Rayleigh number Ra. The gray area represents the slope of the purely convective relation Nu$\sim$Ra$^{1/3}$. The number of plates varies from 3 to 24.

3.1.2 Heat Flux

For the four thermal evolutions obtained with different numbers of plates in Figure 3(e), we compute the heat flux q in a dimensionless form (Nusselt number Nu):

$$\mathrm{Nu} \;=\; q \, \frac{(d_{\mathrm{um}} + d_{\mathrm{lm}})}{k \; (T_m - T_s)} \tag{11}$$

as a function of the Rayleigh number Ra, computed using parameters in Table 1 and Eq. 2 for η_{lm} as a function of T_m:

$$\mathrm{Ra} \;=\; \frac{\alpha \; \rho \; g \; (T_m - T_s) \; (d_{\mathrm{um}} + d_{\mathrm{lm}})^3}{\kappa \; \eta_{\mathrm{lm}}} \tag{12}$$

The very good fit with the classical relation $Nu \sim Ra^{1/3}$ (Figure 3(f)) demonstrates that the force balance governing the MACMA model can reproduce results obtained in numerical or analogical experiments of isoviscous permanent convection in terms of heat transfer (e.g. Howard, 1966; Turcotte & Oxburgh, 1967). As expected for thermal history, a heat loss that depends on mantle temperature and viscosity with this convective scaling results in unacceptably high temperatures in the Archean. We infer that our force balance corresponds to classical parametrizations for permanent convection and can reproduce the Archean thermal catastrophe.

3.2 Mobile Plate Boundaries

We now aim at examining the impact of the plate boundary network mobility on the heat flux evolution and the consequent thermal behavior of the mantle, both on a timescale of a few million years and on the long term. Figure 4 shows tectonic events over 40 Myr and the consequences of these events on the seafloor age and on the local heat flux. The simulation started at 3 Ga with an initial temperature of 1850 K. As in the rest of the study, we consider that a simulation is thermally Earth-like when the present-day temperature is $T_{m_0} = 1625 \pm 25$ K (e.g. Herzberg et al., 2007). The continental strength is here set to $F_{\mathrm{lim}} = 3$ TN.m^{-1}. Figure 4 exhibits plate boundary creations and disappearances together with their consequences on seafloor ages and oceanic heat flux:

A - 1415 Ma: There is one ridge (R1), one subduction (S1) and two continents (C1 and C2). Seafloor ages at the passive margins on the right of C1 and on the left of C2 are soon reaching the critical age for the initiation of subduction ($\tau_{\mathrm{subd}} \approx 152$ Myr for $T = 1746$ K).

B - 1394 Ma: Two new subductions (S2 and S3) were initiated on the borders of continents C1 and C2. As S2 and S3 are both in an extensive configuration (see Figure 1B), new ridges R2 and R3 are created above these subductions. New oceans are expanding around ridges R2 and R3, which results in new zones of high heat flux. Plate 1 and plate 6 (formerly plate 2 in A) are now driven by slab pull and their velocities increase. Old seafloor is thus rapidly consumed. With the increased accretion velocity around R1, the area of young seafloor is extending. These combined effects increase the total heat loss by more than 83% (from 26.7 to 48.9 TW in 20 Myr).

C - 1374 Ma: Continents C1 and C2 collided and subduction S1 disappeared. The former old seafloor at the passive margins of C1 and C2 has now been consumed by subductions S2 and S3. Only seafloor younger than 50 Myr is present, resulting in a globally high heat loss. As the new oceans centered on R2 and R3 are expanding, ages are becoming older and the total heat loss decreases, but at a slower rate than the increase seen between A and B (see Figure 5 for heat flow evolution).

MACMA allows to simulate long term tectonic evolutions of the seafloor age distribution. The heat loss and temperature evolutions over 3 Gyr are shown in Figure 5, including the episodes described in Figure 4. While the heat loss exhibits irregular and large variations, the temperature shows a much smoother evolution. One peak of heat loss variation, shown in the inset in Figure 5b, is analyzed by studying the seafloor age configuration at 6 times (denoted by letters A to F, with A to C already presented in Figure 4).

The increase in heat flow around 1.4 Ga (between A and C) was explained above with Figure 4, where the global lowering of seafloor ages is clearly visible. In the inset of Figure 5b, a slow heat flow decrease can be seen between ages C and D, which is due to seafloor ages getting older at passive margins (on the borders of continent C3) and for overriding plates above subduction zones (left of subduction S2 and right of subduction S3). A more marked low is then seen between D and F (timespan is 30 Myr):

- Between D and E: Ridge R1 collides with the subduction S2. In MACMA, such a collision results in the disappearance of both R1 and S2, replaced by a staple (shown as a small black circle in the panel E of Figure 5c). The small plate located between S2 and R1 disappears. In panel D, young seafloor is being consumed by

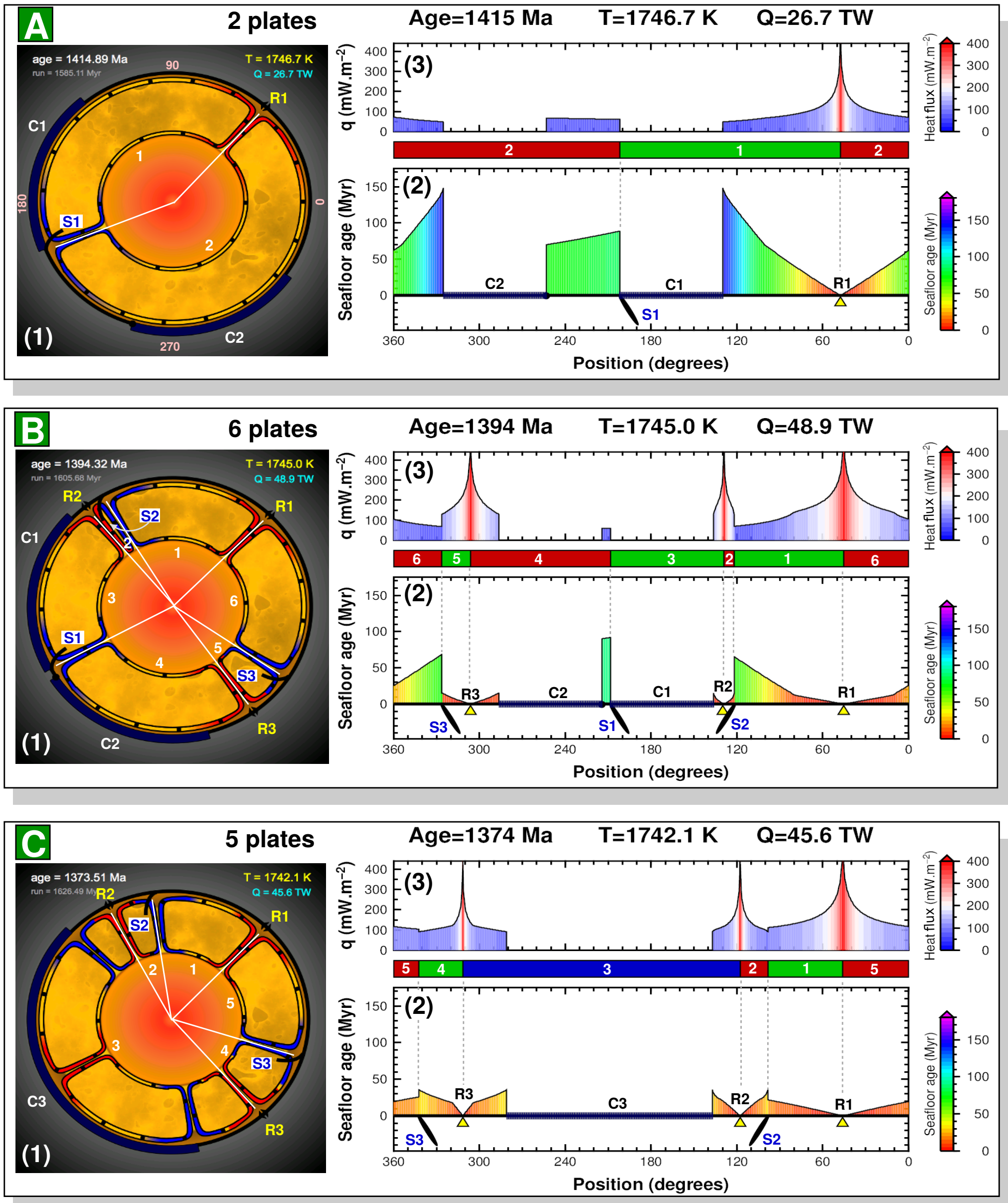

Figure 4. Tectonic plates organization, seafloor ages and heat flux over 40 Myr, for a simulation starting at 3 Ga at a temperature of 1850 K. In each panel (A, B and C) corresponding to three different times, the left portion (1) is the great circle representation in polar coordinates and the right portion shows the seafloor age and the positions of interfaces at the surface (2) and the local heat flux q computed from the seafloor age (3). Positions in degrees are positive counterclockwise (pink numbers in A1). R1, R2 and R3 are ridges; S1, S2 and S3 are subduction zones and C1, C2 and C3 are continents. Positions of plates are shown between two white radii in frame (1) and as colored bars between frames (2) and (3): green, red and blue bars indicate plates respectively moving left, moving right or immobile.

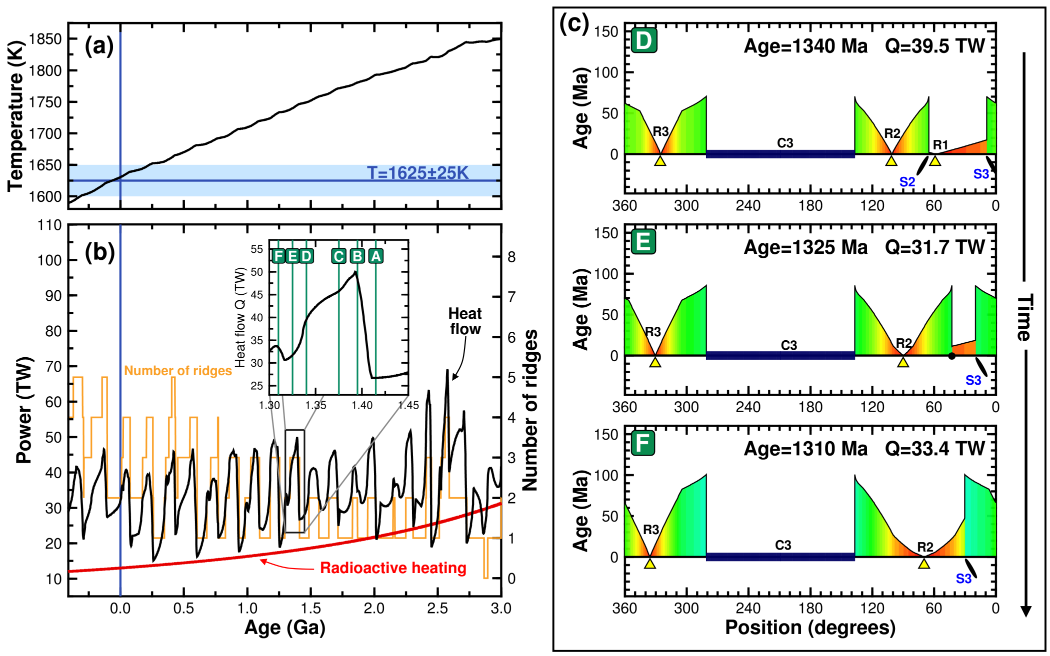

Figure 5. (a) Temperature evolution over 3 Gyr. (b) Total heat flow Q, radioactive heating H and number of ridges as a function of time. The inset is a zoom on the heat flow for ages between 1.30 and 1.45 Ga; (c) Seafloor ages at times D, E and F. The times A, B and C are already described in Figure 4. Color scale for seafloor ages is the same as in Figure 4.

the subduction S3 but it is renewed by seafloor creation at R1. Once R1 disappears, the portion of young seafloor located between the staple and S3 on panel E rapidly vanishes, which accelerates the decrease in heat loss.

- Between E and F: Once the staple was subducted, slab pull at subduction S3 is getting stronger as older seafloor enters the subduction. The plate located between R2 and S3 accelerates, which results in a wider area of young seafloor around R2 and induces the small local increase in heat loss seen in the inset of Figure 5b.

Figures 4 and 5 illustrate how local surface events such as subduction initiations, ridge creations, plate disappearances or changes in seafloor age at the trench can induce important heat flow variations. Not shown in Figures 4 and 5 is the effect of a continental breakup: the result on heat loss is similar to the pattern observed between A and C, with the creation of a new ocean, producing a local pulse of high heat flux. For all cases of heat loss variations that were examined during this study, one or several tectonic rearrangements were observed as the cause of these variations. In Figure 5b, a correlation is clearly observed between the high frequency variations of heat loss and the number of ridges: each ridge creation or disappearance corresponds to an immediate increase or decrease in heat loss, respectively. This short timescale is partly the consequence of our 2D geometry: on Earth, actual heat flux variations are due to both the limited lifespan of plate boundaries and the evolving pattern of the seafloor age distribution on a spherical surface (Labrosse & Jaupart, 2007).

3.3 Comparison to Plate Reconstruction Models

Recent plate reconstructions (e.g. Domeier & Torsvik, 2014; Müller et al., 2016; Vérard et al., 2015; Matthews et al., 2016; Young et al., 2019) give some characteristics of plate tectonics (e.g. plate speed, number of plates, area of subducted material) at most over the last 580 Myr, with increasing incertitude backwards through time. Paleomagnetic and paleogeographic data, as well as compilations of the timing of past orogens, are used by Condie et al. (2015) to estimate "plate" speed, actually limited to large continents' speed, and the rate of continental collisions since 2.5 Ga. We compare the outputs of our model to some of these data sets. We carried out 200 runs with the parameters indicated in Table 1 (reference case), with varying slightly the initial temperature ($T = 1875 \pm 5$ K) and the initial age (3000 ± 50 Myr). The initial number and positions of plate boundaries and continents, as well as the seafloor age distributions, are randomly pulled so that we have a set of 200 different initial conditions, resulting in 200 different thermal histories. Runs were started here with 4 continents (of random sizes), but we also carried out experiments with 1, 2 or 8 initial continents (each done over 50 runs), and the results are equivalent, because continents initially gather in one supercontinent, with the transition from several to one continent lasting around 200 Myr. All the runs yield a present-day temperature equal to 1625±25K. Results are stacked together for each output (temperature, plate RMS speed, continent RMS speed, subduction area flux and number of plates) and we compute percentiles in order to check the possible range of each output. For high mantle temperatures, plate boundaries are fast and colliding with each other before the critical age for subduction initiation is reached anywhere in the model, yielding relatively short phases (10 to 80 Myr) with only one immobile plate, before subduction can be initiated again. As these phases would not occur on the spherical Earth, where the collision between a ridge and a subduction does not lock the full subduction but triple junctions are possible, we filter out these zero-velocity phases from the stacking of plate and continent speeds. Results are shown in Figure 6. For comparison, the results obtained with the same parameters for fixed plate boundaries (6 plates, case (b) in Figure 3) are shown with a thin annoted line. Two individual runs among the 200 are shown in the Supporting Information (Figures S1 and S2).

Our results are generally consistent with the temperature estimate by Herzberg et al. (2010) (Figure 6(a)). For plate speed (Figure 6(b)) and the area of subducted material (Figure 6(d)), we compare our results to the two existing plate reconstruction models extending back into Paleozoic: the model developed at the University of Lausanne (e.g. Vérard et al., 2015) and the models of Müller et al. (2016) (0-230 Ma) and Domeier and Torsvik (2014) (250-410 Ma) combined together by Matthews et al. (2016) and later modified by Young et al. (2019). For plate speed, at the scale of our study, the two models are almost equivalent and our median plate speed is in good agreement with them, although exhbiting a very slightly insufficient slowing down since Mesozoic. This is however not the case for all individual run (see Supporting Information Figures S1 and S2). For the subduction area flux, Vérard et al. (2015) obtain values that are slightly different from their rate of newly accreted material. In our 2D model, the two values are always exactly equal. We therefore plot the data of Vérard et al. (2015) as the average value between their subducted and accreted areas (blue line in Figure 6(d)). The subduction

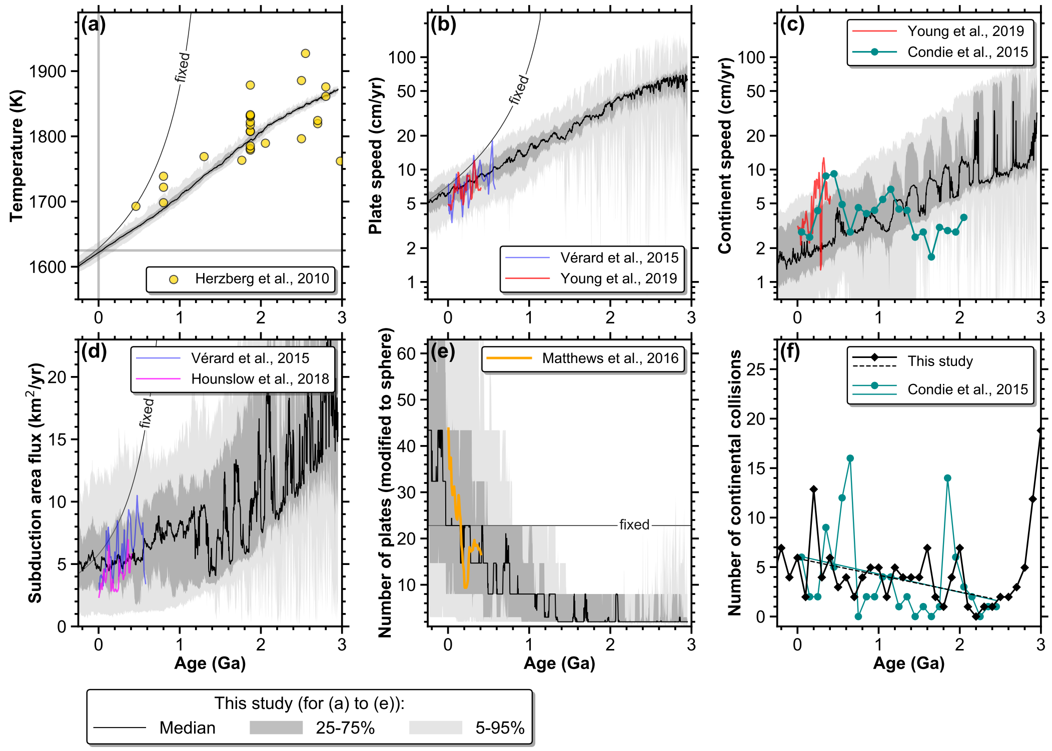

Figure 6. Long term evolutions obtained over 3 Gyr. Solid lines correspond to the median values over 200 stacked runs, while dark and light gray areas are for 25^{th}-75^{th} and 5^{th}-95^{th} percentiles respectively. (a) Temperature evolution compared to Herzberg et al. (2010). (b-c) RMS value of the speeds of all plates (b) and of the continents alone (c) compared to the results of plate reconstructions and models by Vérard et al. (2015) and Young et al. (2019). Continental speed is also compared to results by Condie et al. (2015). Note that (b) and (c) use the same vertical logarithmic scale. (d) Subduction area flux compared to Vérard et al. (2015) and Hounslow et al. (2018). (e) Number of plates (modified to the number on a sphere, using the method described in appendix C) compared to plate reconstructions data by Matthews et al. (2016). (f) Number of collisions for 16 stacked runs (see text for this choice) compared to Condie et al. (2015). The dashed black line and the solid cyan line are linear regressions respectively for their study and our model over the past 2.5 Gyr only (respective slopes: 1.8 and 1.7 collisions/Ga). Results obtained with fixed plate boundaries (case with 6 plates, equivalent to 22.8 plates on the sphere) are also shown (annoted line). Continental speed is then zero and there are no collisions.

area flux given by Hounslow et al. (2018), derived from the plate reconstruction models by Müller et al. (2016) and Domeier and Torsvik (2014) combined together by Matthews et al. (2016), is a bit lower (pink line in Figure 6(d)), illustrating the uncertainty in plate reconstructions. The 25-75% range of our 200 runs encompasses both models.

For the speed of continents, we obtain too low values compared to the evolutions given by Young et al. (2019), especially concerning the peak seen by these authors around 300-370 Ma (see Figure 6(c)). Young et al. get a continent speed at ∼13 cm/yr around 300-330 Ma, which is outside the 5-95% range of our results for all ages younger than 850 Myr. Using paleogeographic and paleomagnetic data, Condie et al. (2015) propose an evolution of "plate speed" (their figure 3), but indicate that their estimate is actually done only on large continents, and therefore we plot it against our results for continent speed, clearly lower than the RMS on all plates (Figure 6(b)). The 5-95% range of our results encompasses their estimate, although very marginally for ages older than 1.5 Gyr and not for their point at 350 Ma. Condie et al. (2015) do not plot the RMS speed of continents as is done by Young et al. (2019) but the weighted-mean (with continents' areas as weights). In Figure 6(c) we use the continent RMS speed for our results. We computed the weighted-mean for comparison: for ages younger than 1 Gyr, the weighted-mean for continental speeds is around 20% lower than the RMS speed, and the difference is negligible for ages older than 1 Gyr, thereby not rendering our results closer to the estimates of Condie et al. (2015). With our approach, the variability of speeds is clearly larger for continents only (Fig. 6(c)) than for the ensemble of plates (Fig. 6(b)); note that the vertical scale is logarithmic. High continental speeds (over 13 cm/yr) in plate reconstructions have been attributed to possible modeling artefacts (e.g. Zahirovic et al., 2015) or discussed as an inadequate choice in the reference frame and in latitude calculations from paleomagnetic data (Condie et al., 2015). Considering the large uncertainty in reconstructions prior to the Mesozoic, the high variability of continental speeds and the simplicity of our model (circular geometry and a unique viscosity for the upper mantle, with no continental lithospheric keels), the moderate discrepancy between our model and continental speed data does not rule out our approach. Future work should include improvements in the implementation of continents (adding continental keels with their specific viscosity for instance).

For the evolution of the number of plates, a direct comparison between our 2D model and actual plate reconstructions on 3D Earth is inadequate. We therefore compute an approximate equivalent number of plates on the sphere using the method described in appendix C and plotted in the Supporting Information (Figure S3). For instance, over the 200 stacked runs, the first quartile, median and third quartile for the present-day number of plates are 4, 6 and 8, which convert to 8.0, 22.8 and 43.3 on the sphere. With this method, our results are in good agreement with the evolution of the number of plates since late Paleozoic given by Matthews et al. (2016) (Figure 6(e)), but this should be taken with caution as it strongly depends on the method used to extrapolate our results to a spherical geometry.

Finally, we compare our results to the evolution of the number of collisions compiled by Condie et al. (2015). Again, our results cannot be directly compared to results on the 2D spherical surface of the Earth. Our 1D Earth's surface contains necessarily less continents, and each continent can only collide with one of its two direct neighboring continents. We adopted the following strategy: Condie et al. (2015) obtain a total of 96 collisions between 2.5 Ga and present-day (see their appendix, part 2, column "Collisional"), while on average, each of our individual run exhibits 6 collisions over this period. We thus added together 16 of our 200 runs, counting the number of collisions per time window of 100 Myr, as is done by Condie et al. (2015), and checked that we had a total of 96 collisions between 2.5 Ga and present-day. Result is shown in Figure 6(f). Between 3 Ga and 2.5 Ga, the steep slope for our study marks the gathering of the initial four continents into one supercontinent, before this continent breaks up and collisions become possible. The general trend for ages younger than 2.5 Gyr is surprisingly similar to the one obtained by Condie et al. (2015), with almost the same linear regression slope. Again, this result strongly depends on the chosen strategy to go from a 1D to a 2D surface, but the increasing collision frequency over time is obtained for any individual run and for the sum of the 200 runs. This is not in contradiction with the decrease in plate speed obtained at the same time over 2.5 Gyr: with an increasing number of plates (and of continents), collisions become more frequent over time even if plates are slowing down.

3.4 Testing MACMA Parameters

Our model is controlled by many parameters (see Table 1) and assessing the individual and interdependent effects of each of them is beyond the scope of the present study. Some parameters were chosen as they correspond to usual estimates and yield accepted present-day plates' speeds (see section 2.1.3). Here we focus on parameters whose values are not precisely known: the mantle activation energy E, the viscosities η_{lm_0}, η_{um_0} and η_{pl_0}, the continental strength F_{lim} and the present-day critical age for subduction initiation τ_{subd_0}. We do not carry a thorough parametric study but vary each parameter around its reference value given in Table 1. The ratio of lower to upper mantle viscosities ($\eta_{\mathrm{lm}_0}/\eta_{\mathrm{um}_0} = 100$) as well as the ratio of oceanic lithosphere to upper mantle viscosities ($\eta_{\mathrm{pl}_0}/\eta_{\mathrm{um}_0} = 250$) are kept constant so that cases hereafter are identified only by the lower mantle viscosity η_{lm_0}.

For this study, we choose the initial mantle temperature so that after 3 Gyr of run the obtained present-day temperature is close to the reference one ($T_{\mathrm{m}_0} = 1625{\pm}25$ K). We present three outputs: the temperature as a function of age, and the plate RMS speed and the number of plates as a function of temperature (Figures 7 and 8). For each parameter, 50 runs are stacked together, and results are sorted into 10 K bins of temperature.

3.4.1 Effect of Parameters Controlling Viscosities

The evolution of the viscosities η_{lm}, η_{um} and η_{pl} as a function of temperature depends on the activation energy E (see Eq. 2). As we study cases that are all yielding the same present-day temperature, E affects the factor by which past viscosities are reduced compared to present ones. We test activation energies ranging from 250 to 450 kJ.mol^{-1}. The values 250 and 450 kJ^{-1} imply that the viscosities are divided by a factor 7.6 and 38.5, respectively, when the temperature is increased by 200 K compared to the present-day one ($T_{\mathrm{m}_0} = 1625$ K). In addition, the present-day lower mantle viscosity η_{lm_0} serves as a reference for all viscosities, and varying η_{lm_0} by a certain factor amounts to multiply all viscosities (lower mantle, upper mantle and oceanic lithosphere), at all temperatures, by the same value. Compared to the present-day reference value ($\eta_{\mathrm{lm}_0} = 5 \times 10^{22}$ Pa.s), we test viscosities multiplied by factors ranging from 1/4 to 4.

Results are presented in Figure 7, both for evolving plate boundaries and for a fixed configuration (2 continents, 6 plates: case (b) in Figure 3, shown with a black solid line in Figure 3(e) and (f)). The thermal runaway backwards in time occurs in the fixed configuration for all tested values of E and η_{lm_0} (Figure 7(a) and (d)). With evolving plate boundaries, all thermal evolutions are consistent with the estimates of (Herzberg et al., 2010). They do not strongly depend on the activation energy E and only slightly on the

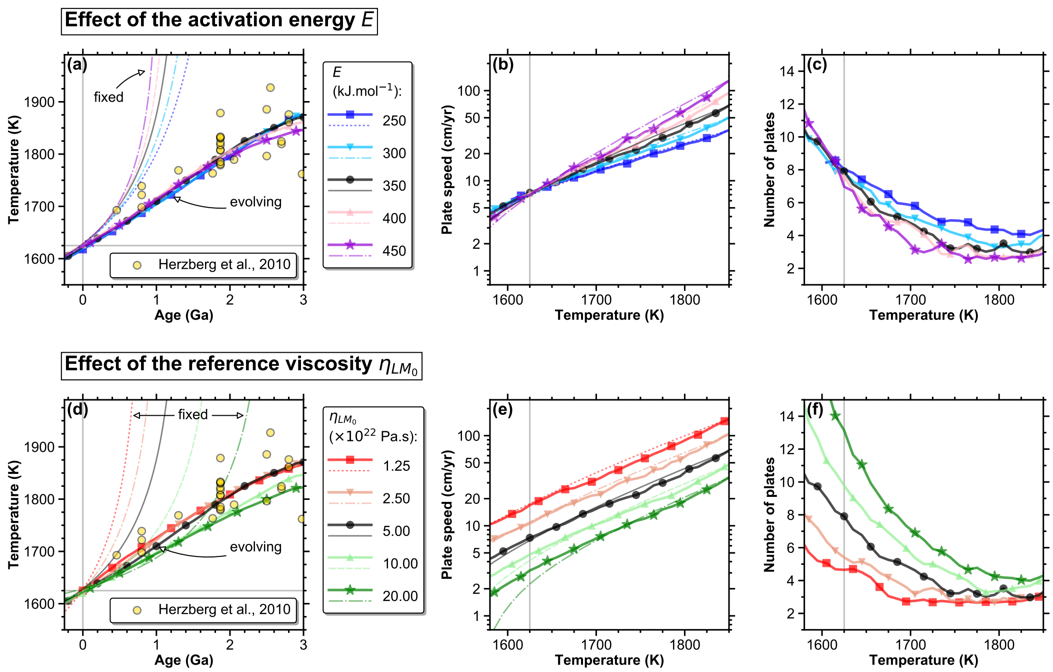

Figure 7. Long term evolution of temperature as a function of age (a and d), average plate RMS speed (b and e) and average number of plates (c and f) as a function of temperature (by bins of 10 K), with varying the activation energy E (a, b and c) and the present-day viscosity η_{lm_0} (d, e and f). Thick lines with symbols are for evolving plate boundaries while thin ones are for fixed boundaries, considering 6 plates (see Figure 3(b)).

present-day reference viscosity η_{lm_0}. However, varying the viscosities, either only in the past when changing E or throughout the full evolution when changing η_{lm_0}, strongly affects the speed of plates: as expected, high viscosities yield lower speeds (see Figure 7(b) and (e)). Speeds obtained with evolving plate tectonics are close to the ones obtained for the same parameters with a fixed configuration.

But with evolving plate tectonics, the number of plates is also affected by a change in the viscosity: a high viscosity implies slower plates, which reaches the critical age for subduction τ_{subd} for a smaller width. The tensive shear force that controls continental break up is also stronger for a higher value of the viscosity, so that continents will break up more easily. A higher viscosity thus results in a larger number of plates (see Figure 7(c) and (f)).

The cooling rate is controlled by the oceanic heat flux, itself computed from the seafloor age distribution. Faster plates, with a fixed size, exhibit young oceanic ages and thus a high heat loss. But with our approach for evolving plate boundaries, viscosities do not affect only the speed of plates but also their size, as can be expected if subduction initiation and ridge creation through continental breakup are phenomena where viscous stresses have to overcome a given yield strength. Varying the viscosities produces two opposite effects: increasing the viscosity slows down plates but decreases their size (i.e. increases their number), so that the average seafloor age does not vary much and the cooling rate is not strongly affected by a change in the viscosity parameters (E or η_{lm_0}). One may note here that temperature evolution alone is not sufficient to assess the effect of physical parameters on mantle cooling dynamics.

3.4.2 Effect of Parameters Controlling Oceanization and Subduction Initiation

The continental strength F_{lim} controls the time needed for continents to breakup (see appendix B). We test values ranging from half the reference one to infinity (continents never break up). τ_{subd_0} is the present-day critical age for subduction initiation and we test values ranging from 140 to 220 Myr. The values 140 and 220 Myr yield a critical age for subduction initiation equal to 106 and 167 Myr, respectively, for a temperature 200 K higher than the present-day one (see Eq. 9). Results are shown in Figure 8.

Varying these two parameters, F_{lim} and τ_{subd_0}, does not modify the plate speed as a function of temperature (see Figure 8(b) and (e): note that lines for evolving or fixed plate boundaries cannot be distinguished), but it strongly affects the average cooling rates. This is due entirely to the change in the geometry of plates: a lower continental strength or a younger critical age for subduction both imply a larger number of plates and plate boundaries at all temperatures. With no change in the plate speed, this necessarily gives overall younger seafloor ages and a more efficient heat loss. For the range of tested parameters here, the obtained thermal evolutions are all compatible with the estimates of Herzberg et al. (2010). τ_{subd_0} and F_{lim} cannot be more constrained by our study. More insight in the mechanisms of oceanization and subduction initiation would be necessary. Subduction initiation probably depends on many surface factors, such as sedimentary loading or variable thickness of the continental crust (e.g. Nikolaeva et al., 2011; Levy & Jaupart, 2012). Similarly, a unique continental strength F_{lim} cannot account for local structural inheritance. Although our parameterization here is simple, we show that

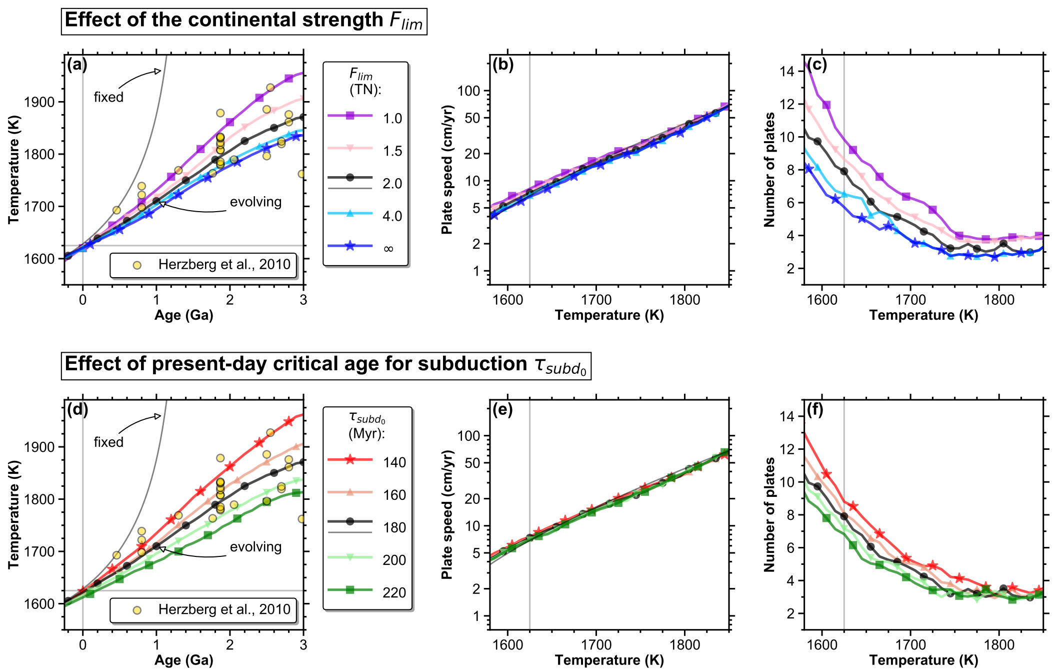

Figure 8. Long term evolution of temperature as a function of age (a and d), plate RMS speed (b and e) and number of plates (c and f) as a function of temperature, with varying the continental strength F_{lim} (a, b and c) and the present-day critical age for subduction initiation τ_{subd_0} (d, e and f).

a fairly wide range of τ_{subd_0} and F_{lim}, that could account for geographical variations, can yield a reasonable thermal history.

4 Discussion

In our 2D model of evolving plate tectonics, plate velocities are controlled by the balance between driving forces (slab pull, ridge push and slab suction) and viscous resistive forces (horizontal mantle drag, vertical viscous shear on slabs and bending dissipation for subduction zones). For individual plates with fixed boundaries (one ridge and one permanent subduction), this force balance yields a scaling for the heat flux as a function of temperature equivalent to the one obtained with isoviscous convection models in a fixed geometry (runaway relation $Nu \sim Ra^{1/3}$, see Figure 3). When plate boundaries are free to move, collide, be created and disappear, plate speed follows approximately the same scaling as a function of temperature as for fixed convective cells (see Figure 7(b, e) and 8(b, e)), but the thermal evolution is completely changed. We obtain a moderate heat loss over 3 Gyr, with large fluctuations on a short timescale that can be linked to rearrangements of plate tessellation (see Figure 5) and a reasonable thermal evolution on a long timescale (Figure 6(a)). In our model, the moderate heat flux obtained even with a strong temperature-dependence of plate speed is to due to the increase in the number of plates over time: a warm mantle in the past implies large plates, and seafloor ages remain thereby sufficiently old to yield a moderate heat loss even in the Archean and early Proterozoic.

The idea of longer and thus less numerous plates in the past may seem counter-intuitive. Recently, Mallard et al. (2016) rather suggested an elongation of plates over time as the mantle cools down, which prompted Matthews et al. (2016) to attribute the smaller number of plates they obtain prior to the Cenozoic (see orange line in Figure 6(e)) to the lack of seafloor preservation which hinders reconstructions of small plates. From 3D spherical models of mantle convection with a visco-pseudoplastic rheology that self-consistently generates plate boundaries, Mallard et al. (2016) observe that a higher yield stress generates longer plates. With our approach, a higher yield stress is equivalent to an older critical age for subduction initiation. In our model, at a given temperature, choosing a higher value of τ_{subd_0} yields a smaller number of plates (see Figure 8(f)), but the number of plates is still increasing with time, which is contrary to the interpretation made by Mallard et al. (2016). Their statistical study is based on a few number of snapshots from steady-state simulations which is not per se a model of Earth's thermal evolution. They infer that with time, the lithosphere becomes comparitively stronger relative to declining mantle forces, and that a colder mantle would therefore correspond to a relative higher yield stress. However, the assertion that mantle forces are declining when the mantle cools down is puzzling, as the decrease of convective vigor over time means that velocities are indeed decreasing, but mantle viscosity is increasing and the latter effect is the stronger of the two for a terrestrial activation energy. Considering that mantle forces can be approximated by the product of the viscosity η and a characteristic velocity U, it can be shown that

$$\frac{\eta U}{\eta_0 U_0} = \left(\frac{\Delta T}{\Delta T_0}\right)^{2/3} \left(\frac{\eta}{\eta_0}\right)^{1/3} \tag{13}$$

with using the classical scaling for convective velocity $U \sim Ra^{2/3}$ (Turcotte & Schubert, 2002). A 200 K increase in temperature compared to present day results in a 2.3-fold decrease of mantle forces ηU (for E=350 kJ.mol^{-1}). As a result, longer plates for a comparatively higher yield stress in simulations by Mallard et al. (2016) are actually also pointing to a smaller number of plates in the past, as is observed by Matthews et al. (2016) and obtained in our study (Figure 6(e)).

It has been argued that the lifetime of passive margins was a proxy for the tempo of plate tectonics (Silver & Behn, 2008; Condie et al., 2015). Bradley (2008) compiled geological and geochemical data in the Phanerozoic and Proterozoic to estimate the lifespan of passive margins over time, and showed that Precambrian passive margins may have survived longer than Phanerozoic ones. Several authors infer that this suggests slower plate tectonics in the past (Korenaga, 2011; Condie et al., 2015), but the geometry of the plate network was not considered: a longer lifespan of tectonic entities such as passive margins is also possible when plates are longer. With fewer plate boundaries, orogenic cycles that destroy passive margins are less frequent, so that even with faster plates in the past, our approach is consistent both with a longer survival of passive margins in the late Archean and Proterozoic and with an increasing number of collisions with time (Figure 6(f)).

We show that surface parameters controlling the oceanization process (continental strength F_{lim}) and subduction initiation (present-day critical age τ_{subd_0}) are governing Earth thermal evolution (Figure 8) in our model because they regulate the geometry of plate tectonics, without affecting plate speeds. On the other hand, parameters controlling the viscosity (reference present-day viscosity η_{lm_0} and activation energy E) have a strong control on plate speed, but almost no effect on thermal evolution because they also have an effect on plate length which opposes the one on plate speed in terms of seafloor age and heat loss (Figure 7). When assessing the validity of a model of Earth thermal evolution, it is thus important to use available constraints not only on temperature, but also on plate speeds and sizes, even if those data are available only through the Phanerozoic.

Future studies should focus on the two processes that create new plate boundaries. Our criterion for subduction initiation may indeed be challenged: numerous processes have been proposed for the onset of subduction (e.g. McKenzie, 1977; Cloetingh et al., 1989; Mueller & Phillips, 1991; Gurnis et al., 2004; Crameri & Kaus, 2010; Nikolaeva et al., 2011; Levy & Jaupart, 2012; Ulvrova et al., 2019) and relying simply on the ratio between the negative buoyancy of the oceanic lithosphere and a fixed yield stress (Eq. 9) does not reflect the complexity of this key terrestrial process. Continental breakup is also simplified in our model, with an approach relying on a parameterized scaling for the diverging force below insulating continents as a function of time and of mantle viscosity.

Recently, Patočka et al. (2020) showed that the role of heat flow coming from the core should not be neglected, while we considered the same cooling rate for the mantle and the core (Eq. 1). A future study should include the non-zero heat flow coming from the core, and a parameterized model of core cooling could be coupled to our model. Our treatment of continents is also a simplification: they are perfectly insulating and their total surface area is fixed. The latter point is not critical here as our simulations start at 3 Ga and many models of continental crust growth predict that the present-day continental fraction was reached in less than 1 Gyr (e.g. Armstrong, 1991; Rosas & Korenaga, 2018). But the possibility of continental growth, with the coeval depletion in radioactive elements, coupled to the subduction rate that can be tracked with our approach, could bring an additional constraint to our model.

The only parameter controlling the evolution of the viscosities in our model so far is temperature (Eq. 2), while water concentration has a non-negligible effect on viscosities (e.g. Hirth & Kohlstedt, 1996; Mei & Kohlstedt, 2000). The possible stiffening effect of dehydration of the oceanic lithosphere can slow down plates and strongly affect Earth's thermal evolution (Korenaga, 2006). The feedback between mantle hydration and heat loss was studied by Crowley et al. (2011) and Korenaga (2011), but with a parameterized approach that does not explicitely address the effect of the viscosity on the geometry of plate tectonics. As individual parametrizations for local processes can be added in our model, testing for the effect of mantle hydration over time through the subduction of hydrated oceanic crust is possible, in order to discuss the feedback between viscosities, plate speeds and plate sizes.

Even though our simple model yields a thermal history consistent with geochemical constraints and plate reconstructions, the additional complexities recently considered to solve the "thermal catastrophe" paradox, such as heat flow from the core (Patočka et al., 2020) and mantle hydration over time (Crowley et al., 2011; Korenaga, 2011) are not ruled out by our approach, but we infer that the effect of those complexities on the geometry of plates should be studied. Studying the control that a parameter exerts on the speed of plates only, without verifying the effect on their geometry, is not sufficient to understand the role of this parameter on Earth's thermal evolution.

5 Conclusion

We propose a model of Earth's thermal history relying on a simple force balance for individual plate speed and on behavioral laws for the motion, creation and destruction of plate boundaries, based on present-day observations. The viscosity of the mantle exerts the main control on plate speeds in our model, as in isoviscous convective cells. This yields a thermal runaway if plates have fixed sizes. With the additional motion of plate boundaries, which collide, disappear and are created when a given yield strength is overcome, we obtain a moderate temperature evolution consistent with geochemical estimates over the past 3 Gyr, an increasing rate of collisions between continents also in agreement with paleogeographic reconstructions since the Archean, and a slowdown of plates and increase in their number that match recent plate reconstructions over the Phanerozoic. We infer that localized surface processes that control the geometry of plate tectonics are key to understand Earth's thermal evolution.

Appendix A Equivalent Viscosities for Resistive Forces

The vertical viscous shear VS on descending slabs is taken into account in the upper mantle only, and the characteristic width of the sheared zone is $d_{\mathrm{um}}/2$ (Grigné et al., 2005), which gives

$$\mathrm{VS} \;=\; -\eta_{\mathrm{um}} \left(\frac{U}{d_{\mathrm{um}}/2} \right) \; \min(Z, d_{\mathrm{um}}). \tag{A1}$$

Writing $\mathrm{VS} = -\eta_{\mathrm{VS}}\, U$ yields

$$\eta_{\mathrm{VS}} \;=\; 2 \left(\frac{\min(Z, d_{\mathrm{um}})}{d_{\mathrm{um}}} \right) \eta_{\mathrm{um}} \tag{A2}$$

where Z is the depth reached by the slab.

For the horizontal mantle drag MD, we consider that the whole mantle is sheared. We denote by U_i the horizontal velocity at the interface between the upper and lower mantle. Considering that the viscous shear is continuous across this interface, we have

$$\eta_{\mathrm{um}} \left(\frac{U - U_i}{d_{\mathrm{um}}} \right) = \eta_{\mathrm{lm}} \left(\frac{U_i}{d_{\mathrm{lm}}} \right). \tag{A3}$$

The horizontal drag is

$$\mathrm{MD} = -\eta_{\mathrm{um}} \left(\frac{U - U_i}{d_{\mathrm{um}}} \right) L \tag{A4}$$

where L is the length of the plate. Eliminating U_i with Eq. A3 and writing $\mathrm{MD} = -\eta_{\mathrm{MD}}\ U$ gives an equivalent viscosity

$$\eta_{\mathrm{MD}} \;=\; \left(\frac{d_{\mathrm{um}}}{\eta_{\mathrm{um}}} + \frac{d_{\mathrm{lm}}}{\eta_{\mathrm{lm}}}\right)^{-1} L. \tag{A5}$$

We use the expression for bending dissipation given by Buffett (2006):

$$\mathrm{B} \;=\; -\frac{2}{3}\,\eta_{pl}\left(\frac{\delta(\tau_{\max})}{R_{\min}}\right)^{3} U \tag{A6}$$

where $\delta(\tau_{\max})$ is the thickness of the lithosphere at the trench, given by equation (3). Writing $\mathrm{B} = -\eta_{\mathrm{B}}\ U$ yields

$$\eta_{\mathrm{B}} \;=\; \frac{2}{3}\left(\frac{\delta(\tau_{\max})}{R_{\min}}\right)^{3}\eta_{\mathrm{pl}}. \tag{A7}$$

Appendix B Divergence Force under Continents

We consider advection created by the warming and consequent upwelling of the mantle under insulating continents. The affected zone has a thickness denoted by b, and a is the width of the continent (see Figure 1C). Hereunder, the excess temperature due to continental insulation and internal heating is denoted by ΔT_h and the advective horizontal velocity under the continent by u_h. Heat conservation, taking into account advection with a uniform velocity u_h under the continent and internal heat H, can be written

$$\rho c_p\left(\frac{d\Delta T_h}{dt} + 2u_h\,\frac{\Delta T_h}{a/2}\right) = H. \tag{B1}$$

Denoting by w_h the vertical velocity below the continent, mass conservation implies $w_h\ (a/2) = u_h b$. The balance between the buoyancy driving force and the viscous shear stress, given by Turcotte and Schubert (2002), is

$$\alpha\rho\ g\Delta T_h\ (a/2)\ b\ w_h = \eta_{\mathrm{um}}\left(\frac{b\ w_h^2}{a/2} + \frac{(a/2)\ u_h^2}{b}\right). \tag{B2}$$

Using mass conservation to eliminate w_h, this yields

$$u_h \;=\; \frac{(a/2)\ \gamma}{2\eta_{\mathrm{um}}}\ \Delta T_h \tag{B3}$$

where γ is a "thermal stress" (in Pa.K^{-1}) given by:

$$\gamma \;=\; \frac{2b\ \alpha\rho g}{\left(\frac{a/2}{b}\right)^{2} + \left(\frac{b}{a/2}\right)^{2}}. \tag{B4}$$

Eq. B1 becomes

$$\frac{d\Delta T_h}{dt} \;+\; \frac{\gamma}{\eta_{\rm um}}\,\Delta T_h^2 \;=\; \frac{H}{\rho c_p}. \tag{B5}$$

With the initial condition $\Delta T_h = 0$ for $t = 0$, the solution is

$$\Delta T_h(t) \;=\; \Delta T_{\rm max}\;\tanh\left(\frac{t}{t_{\rm warm}}\right) \tag{B6}$$

where

$$\Delta T_{\rm max} = \sqrt{\frac{\eta_{\rm um}\;H}{\gamma\;\rho c_p}} \qquad \text{and} \qquad t_{\rm warm} = \sqrt{\frac{\eta_{\rm um}\;\rho c_p}{\gamma\;H}}. \tag{B7}$$

The excess temperature ΔT_h under the continent can reach a maximum equal to $\Delta T_{\rm max}$ and the characteristic warming duration is proportional to $t_{\rm warm}$ (ΔT_h is 76% of $\Delta T_{\rm max}$ for $t = t_{\rm warm}$). The shear tensive force exerted by u_h under the continent is then

$$F(t) \;=\; 2\;\eta_{\rm um}\;\frac{u_h}{b}\;(a/2) \;=\; \gamma\;\Delta T_h(t)\;\frac{(a/2)^2}{b}. \tag{B8}$$

Appendix C Conversion of the Number of Plates from a Circle to a Sphere

For the geometry of MACMA, we denote by $N_{\rm C}$ the number of plates along the circle of radius $R_{\rm E}$. The equivalent number of plates on the sphere of the same radius $R_{\rm E}$ is written as $N_{\rm S}$ hereafter. We consider plates of equal size, defined by the arc angle θ. If there are $N_{\rm C}$ plates in our MACMA model, then this angle is:

$$\theta \;=\; \frac{2\pi}{N_{\rm C}} \tag{C1}$$

For small enough 2D polygonal plates, it is obvious that a larger number $N_{\rm S}$ of plates whose size is described by the arc angle θ can be fitted on the sphere than the number $N_{\rm C}$ for 1D plates of size θ. Here, we consider the 2D plates on the sphere to be spherical equilateral triangles, with sides' angles equal to θ and vertices' angles denoted by α. The relation between sides (θ) and vertices (α) angles is

$$\cos(\alpha) \;=\; \frac{\cos(\theta) \;-\; \cos^2(\theta)}{\sin^2(\theta)} \tag{C2}$$

The surface area of each triangle is $A \;=\; R_{\rm E}^2\,\big(3\alpha - \pi\big)$, so that the number of triangles that can fitted on the sphere is

$$N_{\rm S} \;=\; \frac{4\pi\;R_{\rm E}^2}{A} \;=\; \frac{4\pi}{(3\alpha - \pi)} \tag{C3}$$

The conversion from the number of plates $N_{\rm C}$ on the circle to $N_{\rm S}$ on the sphere is thus done this way: we compute the average arc angle θ from Eq.C1, then deduce the vertices' angle α of triangular plates on the sphere (Eq. C2) and finally compute $N_{\rm S}$ from

Eq. C3. Note that Eq. C2 is valid only for $\alpha < 2\pi/3$, which corresponds to $N_{\rm C} > 3$ (Eq. C1), so that for $N_{\rm C} \leq 3$ we use $N_{\rm S} = N_{\rm C}$ (see Supporting Information Figure S3).

This conversion is a rough approximation, as we consider equal-sized plates with a simple unique geometry. Another choice for this geometry on the sphere would obviously yield another result. We chose triangles for the simplicity of the conversion and because a sphere can be entirely tiled by equilateral spherical triangles, which is not the case with spherical caps for instance. The purpose here is only to transform our circular geometry to a spherical estimate that can be compared to actual plate reconstructions.

Acknowledgments

This work was supported by CNRS-INSU Syster program. The code MACMA will be made available on a repository prior to publication, as well as stacked results used to plot Figures 6 to 8. For submission now, they are given as a dataset in the Supporting Information (DS1).

References

Abbott, D., Burgess, L., & Longhi, J. (1994). An empirical thermal history of the earth's upper mantle. *J. Geohys. Res.*, *99*, 13,835–13,850.

Argus, D., Gordon, R., & DeMets, C. (2011). Geologically current motion of 56 plates relative to the nonetrotation reference frame. *Geochem. Geophys. Geosyst.*, *12*(11), Q11001. doi: 10.1029/2011GC003751

Armstrong, R. L. (1991). The persistent myth of crustal growth. *Australian Journal of Earth Sciences*, *38*(5), 613–630. doi: 10.1080/08120099108727995

Behr, W. M., & Becker, T. W. (2018). Sediment control on subduction plate speeds. *Earth and Planetary Science Letters*, *502*, 166–173. doi: 10.1016/j.epsl.2018.08.057

Bradley, D. (2008). Passive margins through earth history. *Earth-Science Rev.*, *91*, 1-26. doi: 10.1016/j.earscirev.2008.08.001

Buffett, B. (2006). Plate force due to bending at subduction zones. *J. Geophys. Res.*, *111*(B09405). doi: 10.1029/2006JB004295

Butler, S., & Peltier, W. (2002). Thermal evolution of Earth: Models with time-dependent layering of mantle convection which satisfy the urey ratio constraint. *J. Geophys. Res.*, *107*.

Čížková, H., van den Berg, A. P., Spakman, W., & Matyska, C. (2012). The viscosity of Earth's lower mantle inferred from sinking speed of subducted lithosphere. *Physics of the Earth and Planetary Interiors*, *200-201*, 56–62. doi: 10.1016/j.pepi.2012.02.010

Cloetingh, S., Wortel, R., & Vlaar, N. (1989). On the initiation of subduction zones. *Pure Appl. Geophys.*, *129*, 7–25.

Coltice, N., Phillips, B., Bertrand, H., Ricard, Y., & Rey, P. (2007). Global warming of the mantle at the origin of flood basalts over supercontinents. *Geology*, *35*, 391–394. doi: 10.1130/G23240A.1

Combes, M., Grigné, C., Husson, L., Conrad, C., Le Yaouanq, S., Parenthoën, M., ... Tisseau, J. (2012). Multiagent simulation of evolutive plate tectonics applied to the thermal evolution of the Earth. *Geochem. Geophys. Geosyst.*, *13*(5). doi: 10.1029/2011GC004014

Condie, K., Pisarevsky, S., Korenaga, J., & Gardoll, S. (2015). Is the rate of supercontinent assembly changing with time? *Precambrian Res.*, *259*, 278-289. doi: 10.1016/j.precamres.2014.07.015

Conrad, C., & Hager, B. (1999). The thermal evolution of the Earth with strong subduction zones. *Geophys. Res. Lett.*, *26*, 3041–3044.

Conrad, C., & Lithgow-Bertelloni, C. (2002). How mantle slabs drive plate tectonics. *Science*, *298*(5591), 207. doi: 10.1126/science.1074161

Conrad, C., & Lithgow-Bertelloni, C. (2004). The temporal evolution of plate driving forces: Importance of "slab suction" versus "slab pull" during the cenozoic. *J. Geophys. Res.*, *109*(B10407). doi: 10.1029/2004JB002991

Crameri, F., & Kaus, B. J. (2010). Parameters that control lithosphericscale thermal localization on terrestrial planets. *Geophys. Res. Lett.*, *37*(L09308). doi: 10.1029/2010GL042921

Crowley, J. W., Gérault, M., & O'Connell, R. J. (2011). On the relative influence of heat and water transport on planetary dynamics. *Earth and Planetary Science Letters*, *310*(3), 380–388. doi: 10.1016/j.epsl.2011.08.035

Davies, G. (1980). Thermal histories of convective Earth models and constraints on radiogenic heat production in the Earth. *J. Geophys. Res.*, *85*, 2517–2530.

Domeier, M., Doubrovine, P. V., Torsvik, T. H., Spakman, W., & Bull, A. L. (2016).

Global correlation of lower mantle structure and past subduction. *Geophysical Research Letters*, *43*(10), 4945–4953. doi: 10.1002/2016GL068827

Domeier, M., & Torsvik, T. (2014). Plate tectonics in the late paleozoic. *Geoscience Frontiers*, *5*, 303-350. doi: 10.1016/j.gsf.2014.01.002

Evans, D. A. D., Li, Z. X., & Murphy, J. B. (2016). Four-dimensional context of Earth's supercontinents. *Geological Society, London, Special Publications*, *424*(1), 1. doi: 10.1144/SP424.12

Faccenda, M., & Dal Zilio, L. (2017). The role of solid–solid phase transitions in mantle convection. *Lithos*, *268-271*, 198–224. doi: 10.1016/j.lithos.2016.11.007

Forsyth, D., & Uyeda, S. (1975). On the relative importance of the driving forces of plate motion. *Geophys. J. R. Astron. Soc.*, *43*, 163–200.

Gerardi, G., Ribe, N. M., & Tackley, P. J. (2019). Plate bending, energetics of subduction and modeling of mantle convection: A boundary element approach. *Earth Planet. Sci. Lett.*, *515*, 47-57. doi: 10.1016/j.epsl.2019.03.010

Gerya, T. V., & Meilick, F. I. (2011). Geodynamic regimes of subduction under an active margin: effects of rheological weakening by fluids and melts. *Journal of Metamorphic Geology*, *29*(1), 7–31. doi: 10.1111/j.1525-1314.2010.00904.x

Goes, S., Capitanio, G., Morra, G., Seton, M., & Giardini, D. (2011). Signatures of downgoing plate-buoyancy driven subduction in cenozoic plate motions. *Phys. Earth Planet. Int.*, *184*, 1–13.

Griffiths, R., Hackney, R., & van der Hilst, R. (1995). A laboratory investigation of effects of trench migration on the descent of subducted slab. *Earth Planet. Sci. Lett.*, *133*, 1–17.

Grigné, C., & Labrosse, S. (2001). Effects of continents on Earth cooling: thermal blanketing and depletion in radioactive elements. *Geophys. Res. Lett.*, *28*, 2707-2710.

Grigné, C., Labrosse, S., & Tackley, P. J. (2005). Convective heat transfer as a function of wavelength. Implications for the cooling of the Earth. *J. Geophys. Res.*, *110*.

Grigné, C., Labrosse, S., & Tackley, P. J. (2007). Convection under a lid of finite conductivity: heat flux scaling and application to continents. *J. Geophys. Res.*, *112*.

Guillou, L., & Jaupart, C. (1995). On the effect of continents on mantle convection. *J.Geophys.Res.*, *100*, 24,217-24,238.

Guillou-Frottier, L., Buttles, J., & Olson, P. (1995). Laboratory experiments on the structure of subducted lithosphere. *Earth Planet. Sci. Lett.*, *133*, 19–34.

Gurnis, M. (1988). Large-scale mantle convection and the aggregation and dispersal of supercontinents. *Nature*, *332*, 695–699.

Gurnis, M., Hall, C., & Lavier, L. (2004). Evolving force balance during incipient subduction. *Geochem. Geophys. Geosyst.*, *5*(Q07001). doi: 10.1029/2003GC000681

Heron, P., & Lowman, J. P. (2014). The impact of Rayleigh number on assessing the significance of supercontinent insulation. *J. Geophys. Res.*, *119*, 711-733. doi: 10.1002/2013JB010484

Herzberg, C., & Asimow, P. (2015). PRIMELT3 MEGA.XLSM software for primary magma calculation: Peridotite primary magma MgO contents from the liquidus to the solidus. *Geochem. Geophys. Geosyst.*, *16*, 563-578. doi: 10.1002/2014GC005631

Herzberg, C., Asimow, P., Arndt, N., Fitton, F., Cheadle, M., & Saunders, A. (2007). Temperatures in ambient mantle and plumes: Constraints from basalts, picrites, and komatiites. *Geochem. Geophys. Geosys..*, *8*(Q02006). doi: 10.1029/2006GC001390

Herzberg, C., Condie, K., & Korenaga, J. (2010). Thermal history of the earth and its petrological expression. *Earth Planet. Sci. Lett.*, *292*(1), 79–88.

Hirth, G., & Kohlstedt, D. (1996). Water in the oceanic upper mantle: implications for rheology, melt extraction and the evolution of the lithosphere. *Earth Planet. Sci. Lett.*, *144*, 93–108. doi: 10.1016/0012-821X(96)00154-9

Holt, A., Buffett, B., & Becker, T. (2015). Overriding plate thickness control on subduction plate curvature. *Geophys. Res. Lett.*. doi: 10.1002/2015GL063834

Honda, S. (1995). A simple parameterized model of earth's thermal history with the transition from layered to whole mantle convection. *Earth and Planetary Science Letters*, *131*(3), 357–369. doi: 10.1016/0012-821X(95)00034-A

Hounslow, M. W., Domeier, M., & Biggin, A. J. (2018). Subduction flux modulates the geomagnetic polarity reversal rate. *Tectonophysics*, *742-743*, 34–49. doi: 10.1016/j.tecto.2018.05.018

Howard, L. (1966). Convection at high Rayleigh number. In H. Gortler (Ed.), *Proceedings of the Eleventh International Congress of Applied Mechanics* (pp. 1109–1115). Springler-Verlag, New York.

Kaneko, T., Nakakuki, T., & Iwamori, H. (2019). Mechanical coupling of motions between the surface plate and the lower mantle slab: Effects of viscosity hill, yield strength, and depth-dependent thermal expansivity. *Physics of the Earth and Planetary Interiors*, *294*, 106274. doi: 10.1016/j.pepi.2019.106274

Karato, S., & Wu, P. (1993). Rheology of the upper mantle: a synthesis. *Science*, *260*, 771-778.

Korenaga, J. (2003). Energetics of mantle convection and the fate of fossil heat. *Geophys. Res. Lett.*, *30*, 1437–1440.

Korenaga, J. (2006). Archean geodynamics and the thermal evolution of the Earth. In K. Benn, J.-C. Mareschal, & K. Condie (Eds.), *Archean Geodynamics and Environments* (Vol. 164, p. 7-32). American Geophysical Union.

Korenaga, J. (2008). Urey ratio and the structure and evolution of earth's mantle. *Rev. Geophys.*, *46*(RG2007). doi: 10.1029/2007RG000241

Korenaga, J. (2010). Scaling of plate tectonic convection with pseudoplastic rheology. *J. Geophys. Res.*, *115*(B11405). doi: 10.1029/2010JB007670

Korenaga, J. (2011). Thermal evolution with a hydrating mantle and the initiation of plate tectonics in the early earth. *J. Geophys. Res.*, *116*(B12403). doi: 10.1029/2011JB008410

Labrosse, S., & Jaupart, C. (2007). Thermal evolution of the Earth: Secular changes and fluctuations of plate characteristics. *Earth Planet. Sci. Lett.*, *260*, 465–481. doi: 10.1016/j.epsl.2007.05.046

Lenardic, A., Cooper, C., & Moresi, L. (2011). A note on continents and the Earth's Urey ratio. *Phys. Earth Planet. Int.*, *188*, 127-130. doi: 10.1016/j.pepi.2011.06.008

Lenardic, A., Moresi, L., Jellinek, A. M., & Manga, M. (2005). Continental insulation, mantle cooling, and the surface area of oceans and continents. *Earth Planet. Sci. Lett.*, *234*, 17–333.

Levy, F., & Jaupart, C. (2012). The initiation of subduction by crustal extension at a continental margin. *Geophys. J. Int.*, *188*, 779-797. doi: 10.1111/j.1365-246X.2011.05303.x

Mallard, C., Coltice, N., Müller, R., & Tackley, P. (2016). Subduction controls the distribution and fragmentation of Earth's tectonic plates. *Nature*. doi: 10.1038/nature17992

Matthews, K. J., Maloney, K. T., Zahirovic, S., Williams, S. E., Seton, M., & Müller, R. D. (2016). Global plate boundary evolution and kinematics since the late paleozoic. *Global and Planetary Change*, *146*, 226 - 250. doi: 10.1016/j.gloplacha.2016.10.002

McDonough, W., & Sun, S.-s. (1995). The composition of the Earth. *Chem.Geol.*, 223-253.

McKenzie, D. P. (1977). The initiation of trenches: A finite amplitude instability. In M. Talwani & W. Pittman (Eds.), *Island arcs, deep sea trenches, and back-arc basins* (Vol. 1, pp. 57–61). AGU, Washington D.C.

Mei, S., & Kohlstedt, D. L. (2000). Influence of water on plastic deformation of olivine aggregates: 1. diffusion creep regime. *Journal of Geophysical Research: Solid Earth*, *105*(B9), 21457–21469. doi: 10.1029/2000JB900179

Mueller, S., & Phillips, R. (1991). On the initiation of subduction. *J. Geophys. Res.*, *96*, 651–665.

Müller, R., Sdrolias, M., Gaina, C., & Roest, W. (2008). Age, spreading rates, and spreading asymmetry of the world's ocean crust. *Geochem. Geophys. Geosys.*, *9*(4). doi: 10.1029/2007GC001743

Müller, R. D., Seton, M., Zahirovic, S., Williams, S. E., Matthews, K. J., Wright, N. M., ... Cannon, J. (2016). Ocean basin evolution and global-scale plate reorganization events since pangea breakup. *Annual Review of Earth and Planetary Sciences*, *44*(1), 107–138. doi: 10.1146/annurev-earth-060115-012211

Nataf, H. C., & Richter, F. (1982). Convection experiments in fluids with highly temperature-dependent viscosity and the thermal evolution of the planets. *Phys. Earth Planet. Sci.*, *29*, 320–329.

Nikolaeva, K., Gerya, T. V., & Marques, F. O. (2011). Numerical analysis of subduction initiation risk along the atlantic american passive margins. *Geology*, *39*(5), 463–466. doi: 10.1130/G31972.1

O'Neill, C., Lenardic, A., Jellinek, A., & Moresi, L. (2009). Influence of supercontinents on deep mantle flow. *Gondwana Res.*, *15*, 276-287. doi: 10.1016/j.gr.2008.11.005

O'Neill, C., Lenardic, A., Moresi, L., Torsvik, T., & Lee, C. (2007). Episodic precambrian subduction. *Earth Planet. Sci. Lett.*, *261*, 552–562.

Parsons, B., & Richter, F. (1980). A relation between the driving force and the geoid anomaly associated with mid-ocean ridges. *Earth Planet. Sci. Lett.*, *51*, 445–450.

Patočka, V., Šrámek, O., & Tosi, N. (2020). Minimum heat flow from the core and thermal evolution of the earth. *Physics of the Earth and Planetary Interiors*, 106457. doi: 10.1016/j.pepi.2020.106457

Pisarevsky, S. A., Elming, S.-Å., Pesonen, L. J., & Li, Z.-X. (2014). Mesoproterozoic paleogeography: Supercontinent and beyond. *Precambrian Research*, *244*, 207–225. doi: 10.1016/j.precamres.2013.05.014

Ribe, N. M. (2010). Bending mechanics and mode selection in free subduction: a thin-sheet analysis. *Geophysical Journal International*, *180*(2), 559–576. doi: 10.1111/j.1365-246X.2009.04460.x

Richter, F. M. (1985). Models for the Archean thermal regime. *Earth Planet. Sci. Lett.*, *73*, 350-260.

Rolf, T., Coltice, N., & Tackley, P. (2012). Linking continental drift, plate tectonics and the thermal state of the Earth's mantle. *Earth Planet. Sci. Lett.*, *351-352*, 134–136. doi: 10.1016/j.epsl.2012.07.011

Rosas, J. C., & Korenaga, J. (2018). Rapid crustal growth and efficient crustal recycling in the early earth: Implications for hadean and archean geodynamics. *Earth and Planetary Science Letters*, *494*, 42–49. doi: 10.1016/j.epsl.2018.04.051

Rudnick, R., & Gao, S. (2003). Composition of the continental crust. In R. Rudnick (Ed.), *Treatise on geochemistry, the crust* (Vol. 3, p. 1-64). New York: Permagon.

Samuel, H., Aleksandrov, V., & Deo, B. (2011). The effect of continents on mantle convective stirring. *Geophysical Research Letters*, *38*(4). doi: 10.1029/2010GL046056

Schubert, G., Stevenson, D., & Cassen, P. (1980). Whole planet cooling and the radiogenic heat source contents of the Earth and the Moon. *J. Geophys. Res.*, *85*, 2531–2538.

Silver, P., & Behn, M. (2008). Intermittent plate tectonics? *Science*, *319*, 85–88.

doi: 10.1126/science.1148397

Sleep, N. (2000). Evolution of the mode of convection within terrestrial planets. *J. Geophys. Res.*, *105, E7*, 17563–17578.

Tozer, D. (1967). Towards a theory of thermal convection in the mantle. In T. Gaskell (Ed.), *The earth's mantle* (pp. 325–353). London, U.K.: Academic Press.

Turcotte, D., & Oxburgh, E. (1967). Finite amplitude convection cells and continental drift. *J. Fluid Mech.*, *28*, 29–42.

Turcotte, D., & Schubert, G. (2002). *Geodynamics.* Cambridge University Press.

Ulvrova, M. M., Coltice, N., Williams, S., & Tackley, P. J. (2019). Where does subduction initiate and cease? a global scale perspective. *Earth and Planetary Science Letters*, *528*, 115836. doi: 10.1016/j.epsl.2019.115836

Van der Meer, D., Spakman, W., van Hinsbergen, D., Amaru, M., & Torsvik, T. (2010). Towards absolute plate motions constrained by lower-mantle slab remnants. *Nat. Geosci.*, *3*, 36–40.

Van der Meer, D., Van Hinsbergen, D., & Spakman, W. (2018). Atlas of the underworld: Slab remnants in the mantle, their sinking history, and a new outlook on lower mantle viscosity. *Tectonophysics*, *723*, 309–448.

Vérard, C., Hochard, C., Baumgartner, P., & Stampfli, G. (2015). Geodynamic evolution of the earth over the phanerozoic: Plate tectonic activity and palaeoclimatic indicators. *Journal of Palaeogeography*, *4*, 167–188. doi: 10.3724/SP.J.1261.2015.00072

Whitehead, J., & Behn, M. (2015). The continental drift convection cell. *Geophys. Res. Lett.*, *42*, 4301-4308. doi: 10.1002/2015GL064480

Wu, B., Conrad, C., Heuret, A., Lithgow-Bertelloni, C., & Lallemand, S. (2008). Reconciling strong slab pull and weak plate bending: The late motion constraint on the strength of mantle slabs. *Earth Planet. Sci. Lett*, *272*, 412–421. doi: 10.1016/j.epsl.2008.05.009

Yoshida, M. (2013). Mantle temperature under drifting deformable continents during the supercontinent cycle. *Geophysical Research Letters*, *40*(4), 681–686. doi: 10.1002/grl.50151

Young, A., Flament, N., Maloney, K., Williams, S., Matthews, K., Zahirovic, S., & Müller, R. D. (2019). Global kinematics of tectonic plates and subduction zones since the late paleozoic era. *Geoscience Frontiers*, *10*(3), 989 - 1013. (Special Issue: Advances in Himalayan Tectonics) doi: 10.1016/j.gsf.2018.05.011

Zahirovic, S., Müller, R., Seton, M., & Flament, N. (2015). Tectonic speed limits from kinematic reconstructions. *Earth Planet. Sci. Lett.*, *418*, 40-52. doi: 10.1016/j.epsl.2015.02.037

Figure 1.

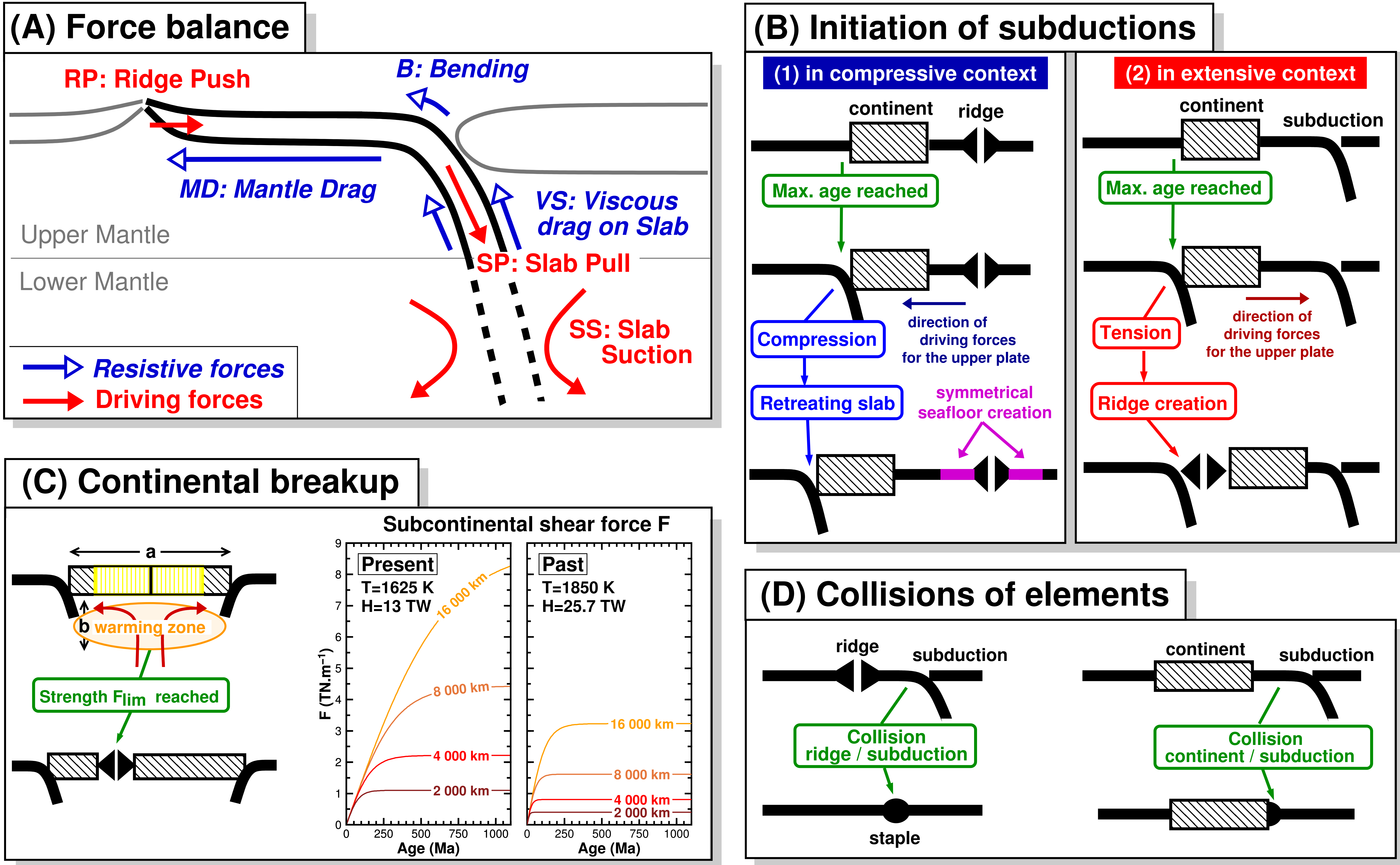

(A) Force balance
RP: Ridge Push
B: Bending
MD: Mantle Drag
VS: Viscous drag on Slab
Upper Mantle
Lower Mantle
SP: Slab Pull
SS: Slab Suction
Resistive forces
Driving forces
(B) Initiation of subductions
(1) in compressive context
continent
ridge
Max. age reached
Compression
direction of driving forces for the upper plate
Retreating slab
symmetrical seafloor creation
(2) in extensive context
continent
subduction
Max. age reached
Tension
direction of driving forces for the upper plate
Ridge creation
(C) Continental breakup
a
b
warming zone
Strength Flim reached
Subcontinental shear force F
Present
T=1625 K
H=13 TW
16 000 km
8 000 km
4 000 km
2 000 km
Past
T=1850 K
H=25.7 TW
16 000 km
8 000 km
4 000 km
2 000 km
F (TN.m⁻¹)
Age (Ma)
0
250
500
750
1000
0
1
2
3
4
5
6
7
8
9
(D) Collisions of elements
ridge
subduction
Collision ridge / subduction
staple
continent
subduction
Collision continent / subduction

Figure 2.

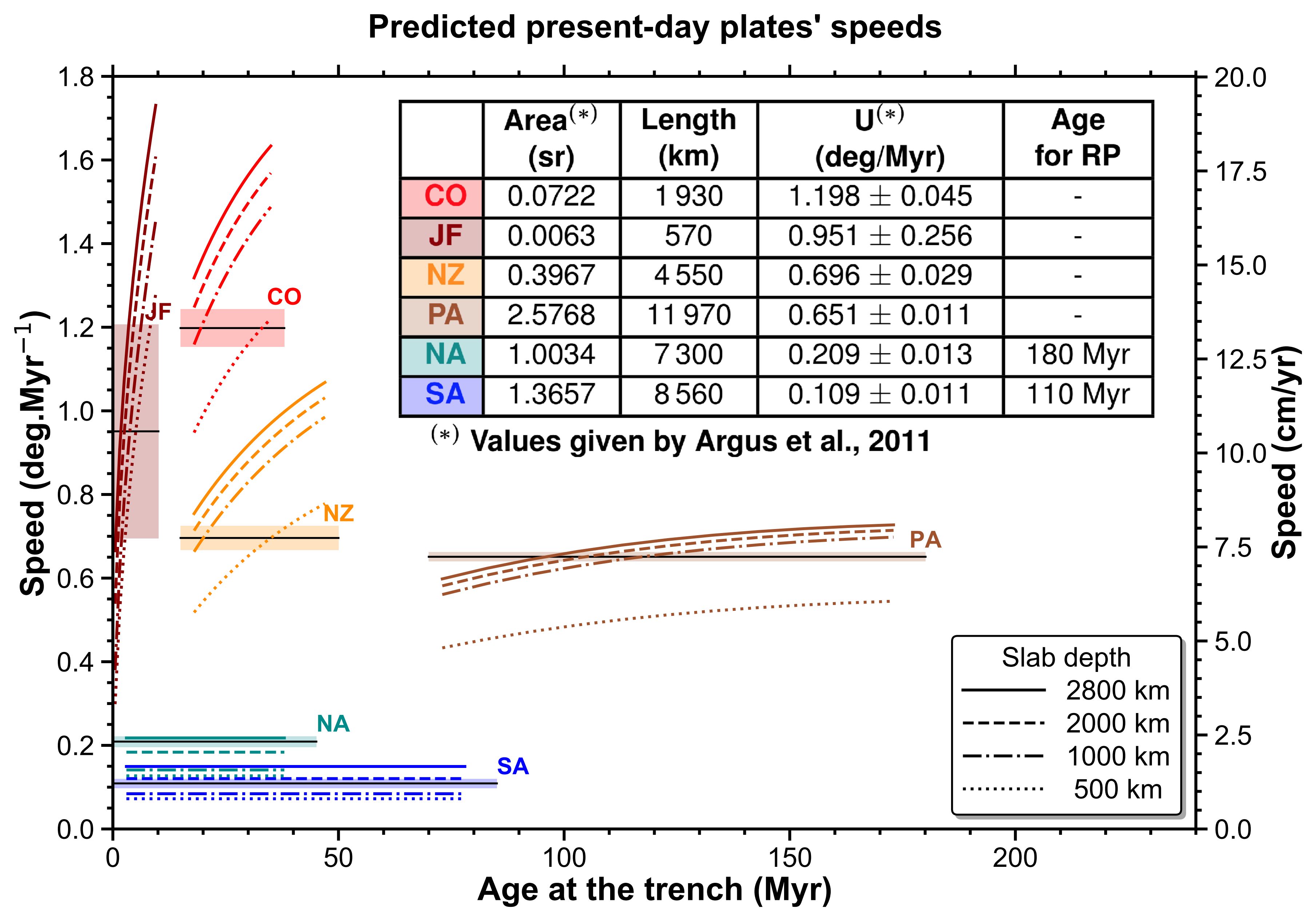
Predicted present-day plates' speeds
Speed (deg.Myr^{-1})
Speed (cm/yr)
Age at the trench (Myr)
0
50
100
150
200
0.0
0.2
0.4
0.6
0.8
1.0
1.2
1.4
1.6
1.8
0.0
2.5
5.0
7.5
10.0
12.5
15.0
17.5
20.0
JF
CO
NZ
PA
NA
SA
	Area$^{(*)}$ (sr)	Length (km)	U$^{(*)}$ (deg/Myr)	Age for RP
CO	0.0722	1 930	1.198 ± 0.045	-
JF	0.0063	570	0.951 ± 0.256	-
NZ	0.3967	4 550	0.696 ± 0.029	-
PA	2.5768	11 970	0.651 ± 0.011	-
NA	1.0034	7 300	0.209 ± 0.013	180 Myr
SA	1.3657	8 560	0.109 ± 0.011	110 Myr
$^{(*)}$ Values given by Argus et al., 2011
Slab depth
2800 km
2000 km
1000 km
500 km

Figure 3.

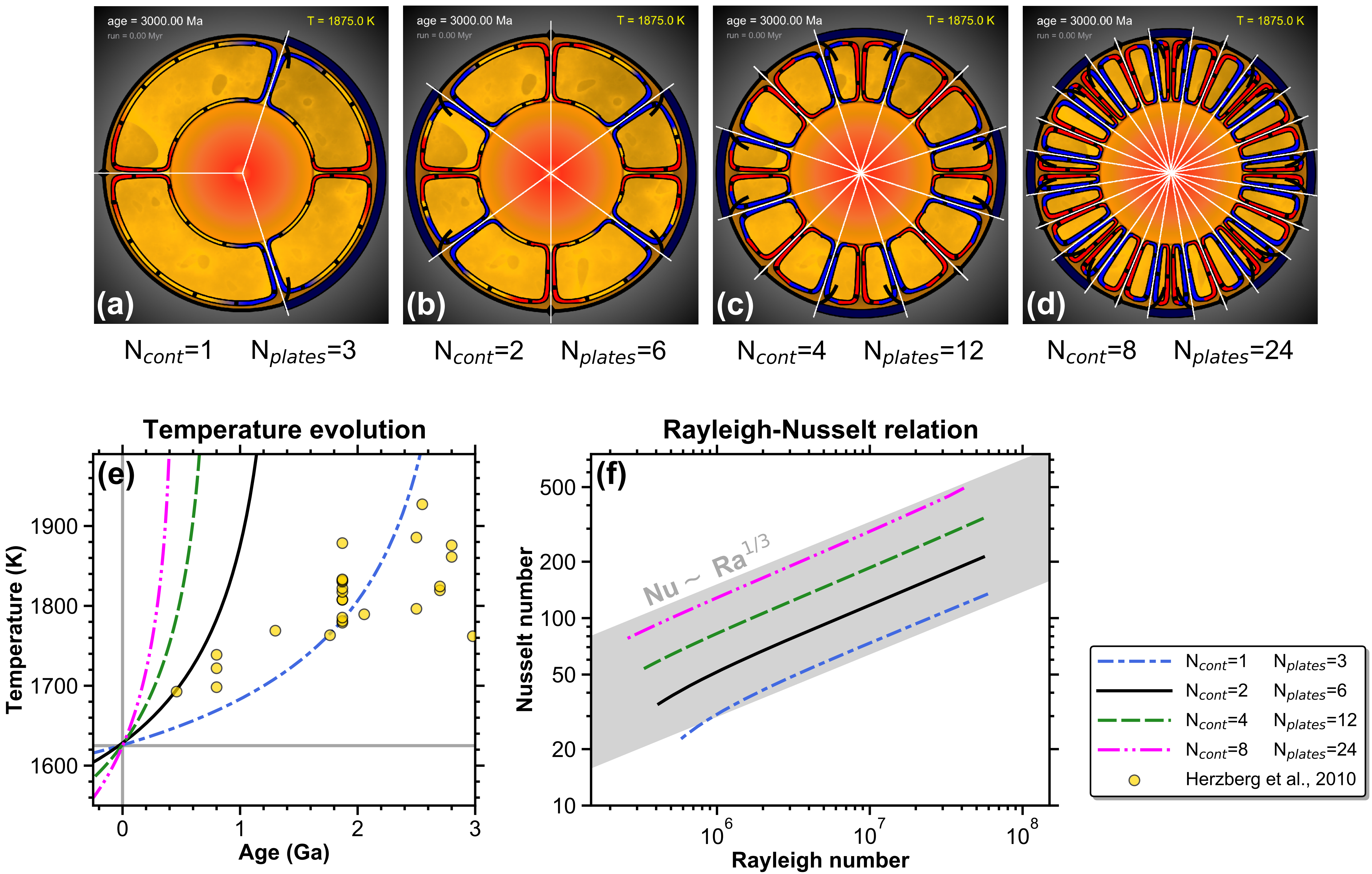

age = 3000.00 Ma
run = 0.00 Myr
T = 1875.0 K
(a)
(b)
(c)
(d)
N$_{cont}$=1 N$_{plates}$=3
N$_{cont}$=2 N$_{plates}$=6
N$_{cont}$=4 N$_{plates}$=12
N$_{cont}$=8 N$_{plates}$=24
Temperature evolution
(e)
Temperature (K)
Age (Ga)
Rayleigh-Nusselt relation
(f)
Nu ~ Ra$^{1/3}$
Nusselt number
Rayleigh number
N$_{cont}$=1 N$_{plates}$=3
N$_{cont}$=2 N$_{plates}$=6
N$_{cont}$=4 N$_{plates}$=12
N$_{cont}$=8 N$_{plates}$=24
Herzberg et al., 2010

Figure 4.

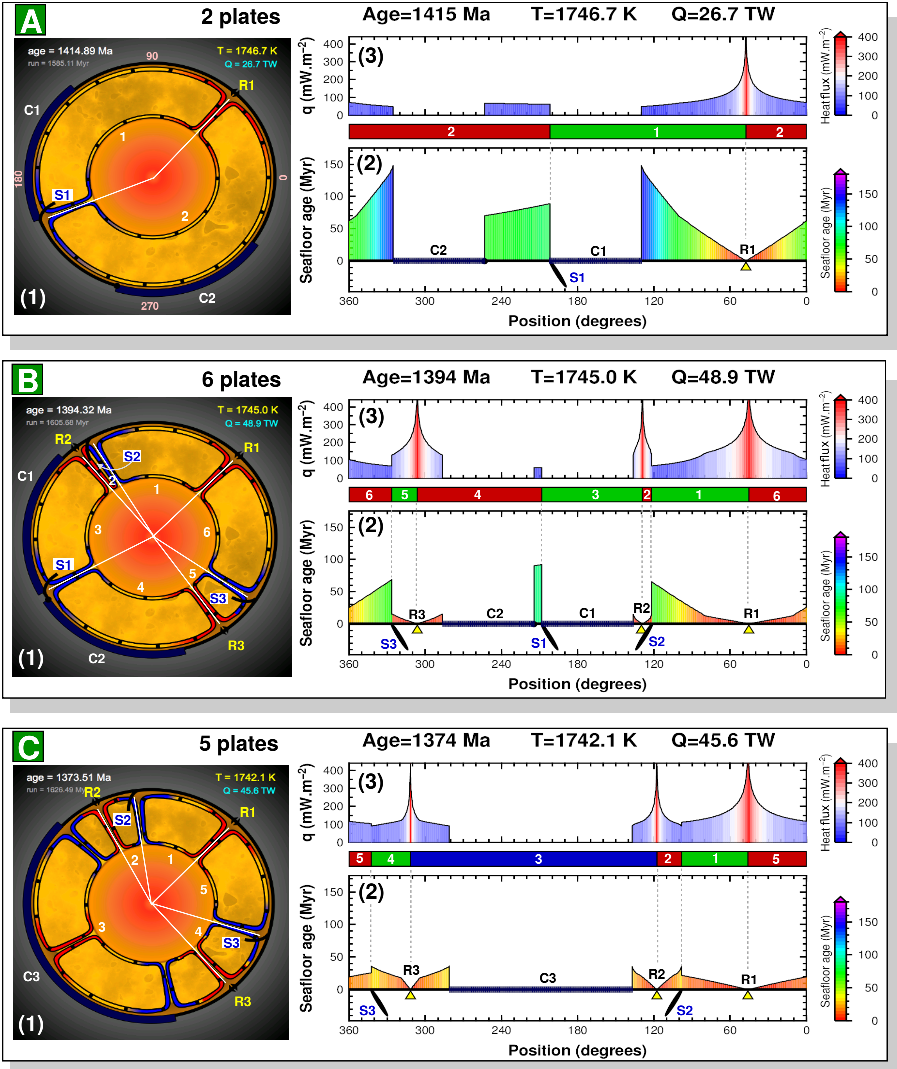
A
2 plates
Age=1415 Ma
T=1746.7 K
Q=26.7 TW
age = 1414.89 Ma
run = 1585.11 Myr
T = 1746.7 K
Q = 26.7 TW
R1
C1
S1
C2
(1)
(2)
(3)
q (mW.m⁻²)
Seafloor age (Myr)
Position (degrees)
Heat flux (mW.m⁻²)
B
6 plates
Age=1394 Ma
T=1745.0 K
Q=48.9 TW
age = 1394.32 Ma
run = 1605.68 Myr
T = 1745.0 K
Q = 48.9 TW
R1
R2
R3
S1
S2
S3
C1
C2
C
5 plates
Age=1374 Ma
T=1742.1 K
Q=45.6 TW
age = 1373.51 Ma
run = 1626.49 Myr
T = 1742.1 K
Q = 45.6 TW
R1
R2
R3
S2
S3
C3

Figure 5.

(a)
Temperature (K)
1850
1800
1750
1700
1650
1600
T=1625±25K
(b)
Power (TW)
110
100
90
80
70
60
50
40
30
20
10
Number of ridges
Heat flow
Radioactive heating
Heat flow Q (TW)
F E D C B A
1.30 1.35 1.40 1.45
0.0 0.5 1.0 1.5 2.0 2.5 3.0
Age (Ga)
(c)
D
Age=1340 Ma Q=39.5 TW
E
Age=1325 Ma Q=31.7 TW
F
Age=1310 Ma Q=33.4 TW
Age (Ma)
R1
R2
R3
C3
S2
S3
360 300 240 180 120 60 0
Position (degrees)
Time

Figure 6.

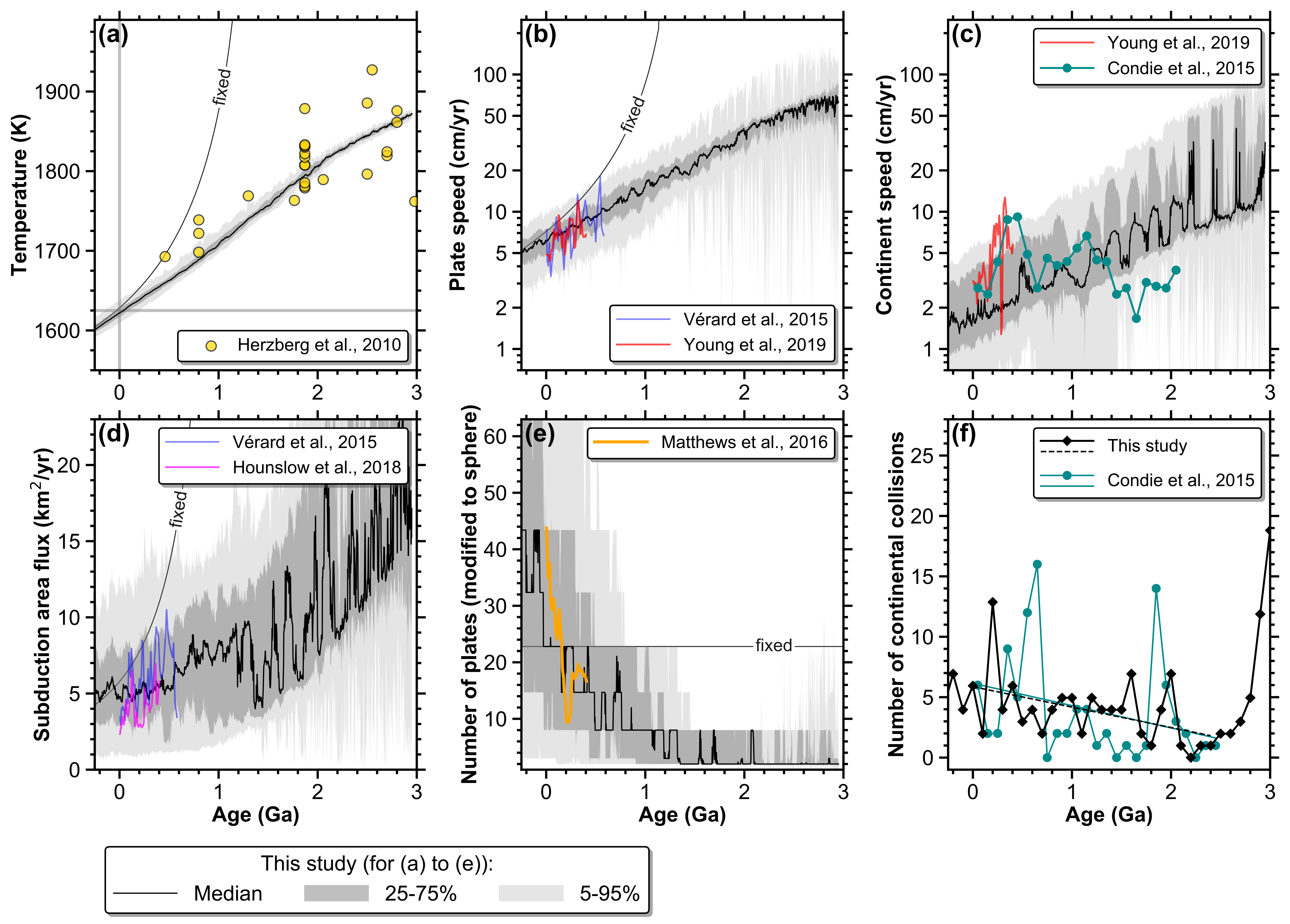
(a)
Temperature (K)
fixed
Herzberg et al., 2010
(b)
Plate speed (cm/yr)
fixed
Vérard et al., 2015
Young et al., 2019
(c)
Continent speed (cm/yr)
Young et al., 2019
Condie et al., 2015
(d)
Subduction area flux (km^2/yr)
fixed
Vérard et al., 2015
Hounslow et al., 2018
(e)
Number of plates (modified to sphere)
fixed
Matthews et al., 2016
(f)
Number of continental collisions
This study
Condie et al., 2015
Age (Ga)
Age (Ga)
Age (Ga)
This study (for (a) to (e)):
Median
25-75%
5-95%

Figure 7.

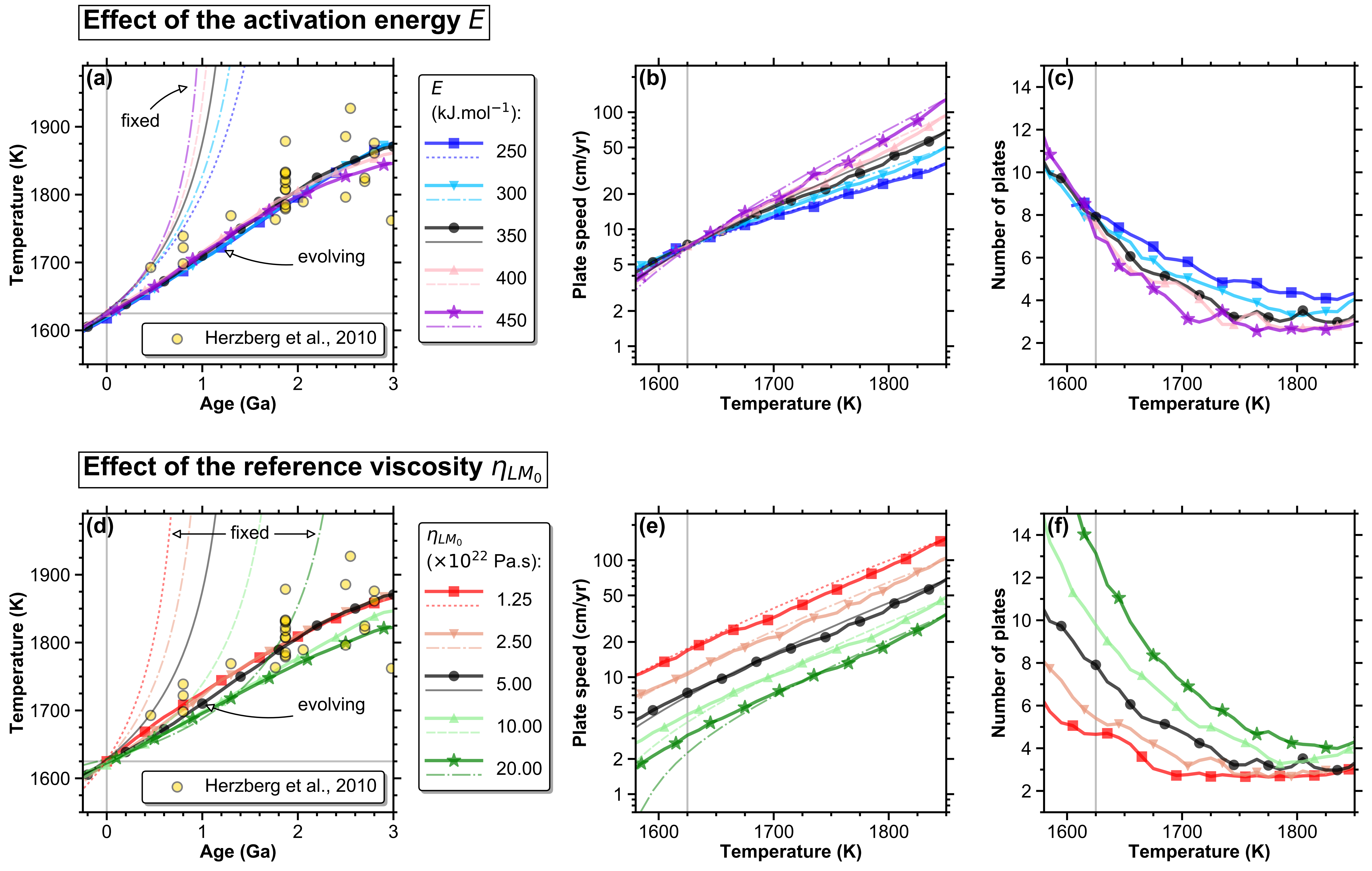

Effect of the activation energy E
(a)
fixed
evolving
Herzberg et al., 2010
Age (Ga)
Temperature (K)
E
(kJ.mol^{-1}):
250
300
350
400
450
(b)
Plate speed (cm/yr)
Temperature (K)
(c)
Number of plates
Temperature (K)
Effect of the reference viscosity η_{LM_0}
(d)
fixed
evolving
Herzberg et al., 2010
Age (Ga)
Temperature (K)
η_{LM_0}
($\times 10^{22}$ Pa.s):
1.25
2.50
5.00
10.00
20.00
(e)
Plate speed (cm/yr)
Temperature (K)
(f)
Number of plates
Temperature (K)

Figure 8.

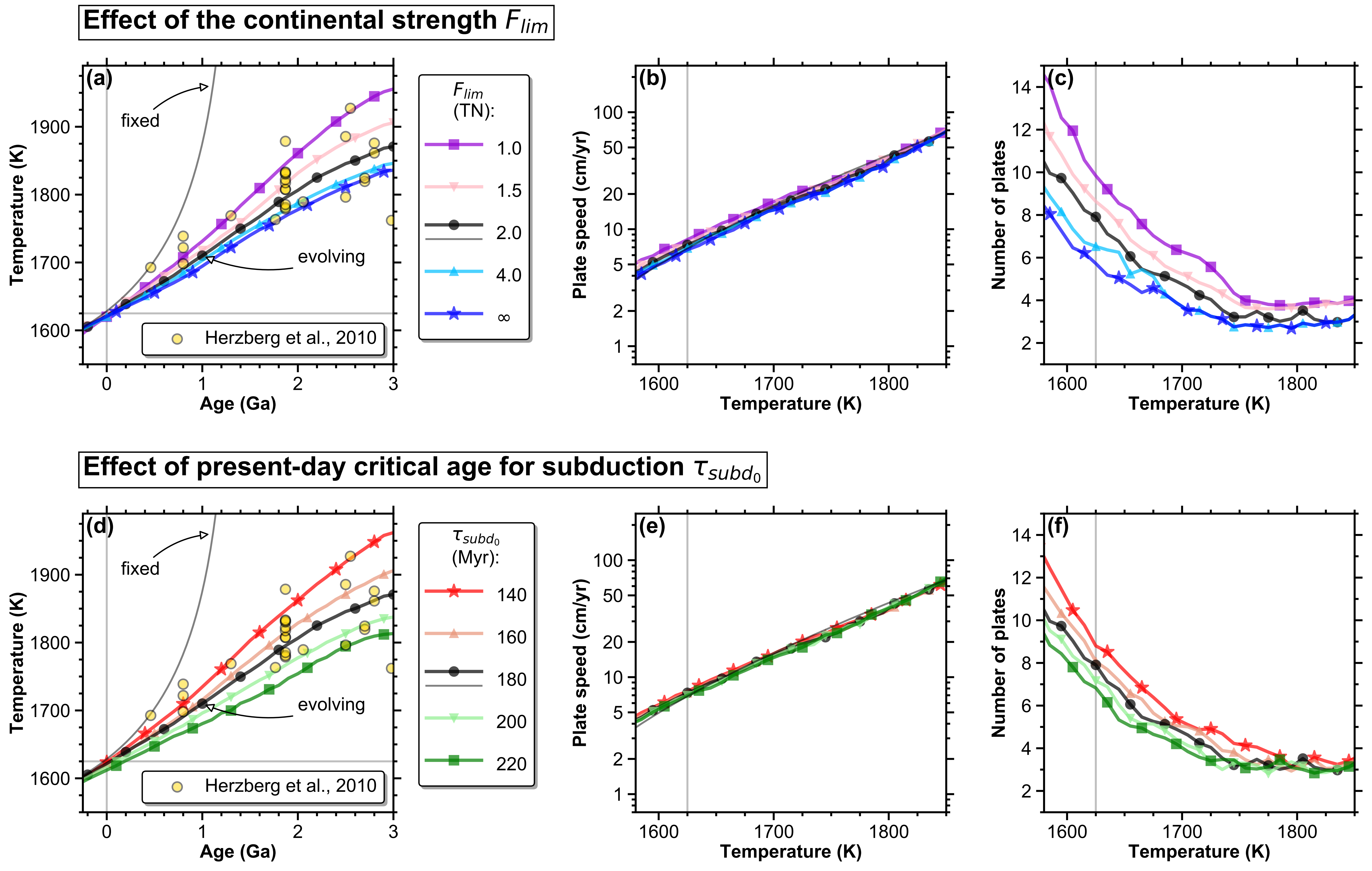

Effect of the continental strength F_{lim}
(a)
(b)
(c)
fixed
evolving
Herzberg et al., 2010
Temperature (K)
Age (Ga)
Plate speed (cm/yr)
Number of plates
Temperature (K)
F_{lim} (TN):
1.0
1.5
2.0
4.0
∞
Effect of present-day critical age for subduction τ_{subd_0}
(d)
(e)
(f)
fixed
evolving
Herzberg et al., 2010
Temperature (K)
Age (Ga)
Plate speed (cm/yr)
Number of plates
Temperature (K)
τ_{subd_0} (Myr):
140
160
180
200
220